

The Rap GTPase Activator *Drosophila* PDZ-GEF Regulates Cell Shape in Epithelial Migration and Morphogenesis[∇]

Benjamin Boettner and Linda Van Aelst*

Cold Spring Harbor Laboratory, Watson School of Biological Sciences, 1 Bungtown Road, Cold Spring Harbor, New York 11724

Received 16 July 2007/Returned for modification 20 August 2007/Accepted 30 August 2007

Epithelial morphogenesis is characterized by an exquisite control of cell shape and position. Progression through dorsal closure in *Drosophila* gastrulation depends on the ability of Rap1 GTPase to signal through the adherens junctional multidomain protein Canoe. Here, we provide genetic evidence that epithelial Rap activation and Canoe effector usage are conferred by the *Drosophila* PDZ-GEF (dPDZ-GEF) exchange factor. We demonstrate that dPDZ-GEF/Rap/Canoe signaling modulates cell shape and apicolateral cell constriction in embryonic and wing disc epithelia. In dPDZ-GEF mutant embryos with strong dorsal closure defects, cells in the lateral ectoderm fail to properly elongate. Postembryonic dPDZ-GEF mutant cells generated in mosaic tissue display a striking extension of lateral cell perimeters in the proximity of junctional complexes, suggesting a loss of normal cell contractility. Furthermore, our data indicate that dPDZ-GEF signaling is linked to myosin II function. Both dPDZ-GEF and *cno* show strong genetic interactions with the myosin II-encoding gene, and myosin II distribution is severely perturbed in epithelia of both mutants. These findings provide the first insight into the molecular machinery targeted by Rap signaling to modulate epithelial plasticity. We propose that dPDZ-GEF-dependent signaling functions as a rheostat linking Rap activity to the regulation of cell shape in epithelial morphogenesis at different developmental stages.

Epithelial morphogenetic processes constitute genetically programmed cell movement or tissue growth that shapes the developing embryo or organ. Such processes entail alterations in tissue shape that are brought about by a variety of different cellular mechanisms, including cell adhesion, cell contractility, cell intercalation, and polarized cell division (3, 27, 56). Concurrently, the integrity of the epithelium has to be maintained at all times. The dorsal closure (DC) process late in *Drosophila* gastrulation has proven to be a superb system with which to study the signaling pathways and mechanical alterations involved in cell shape changes. DC is initiated after the germ band has retracted and the transient amnioserosa is dorsally exposed. Following initiation, the bilateral ectoderm sweeps over the amnioserosa in the dorsal direction to finally engage in zippering at the dorsal midline. In this manner the embryo is tightly sealed. This process, both in terms of genetic contributions and its physiological aspects, is highly reminiscent of the closure of an epithelial wound after a mechanical insult (reviewed in reference 39). The sequence of events that comprises DC is accompanied by dramatic cell shape changes in the contributing tissues. Ectodermal cells elongate along the dorsal-ventral axis, and while gradually spreading over the space occupied by the shrinking amnioserosa, they morph substantially from a thick- to a thin-layered epithelium (29, 39). In contrast, the differentiation of imaginal disc epithelia is driven largely by the orchestration of the growth and orientation of cell division. Newly born cells have to adopt and maintain a well-defined position in the epithelium and adjust their shape to the requirements of their environment. The shape of indi-

vidual cells critically depends on the polarity, adhesion, and tension parameters that govern their neighbors (8, 16, 23).

Cell shape changes in DC and other epithelial migration events are driven largely by nonmuscle myosin, also referred to as myosin II (MyoII), which generates mechanical force at the leading edge, the lateral ectoderm, and the amnioserosa by modulating contractile events proximal to cell-cell adhesion complexes (13). In proliferating and differentiating epithelia, MyoII provides general cell tension and is involved in the establishment of compartment boundaries (38). MyoII assembly and activity are tightly controlled by signal transduction pathways, among which the Rho GTPase/Rho-kinase pathway is the best studied (11, 43, 55). However, recent studies have documented the existence of Rho-independent pathways that regulate MyoII assembly and contractility. For instance, in the slime mold *Dictyostelium*, multiple MyoII heavy-chain kinases have been identified that affect MyoII assembly but function without a regulatory input from the Rho pathway (49, 62). In *Xenopus* gastrulation, a pathway involving the Shroom protein and the small GTPase Rap1 likely engages MyoII in the closure of the neural tube (17, 20, 21). The precise operational mechanisms of these pathways largely remain to be deciphered, but they underscore that epithelial cell shape can be regulated by both Rho-dependent and Rho-independent means.

The Rap GTPases have emerged as key regulators not only of integrin-mediated adhesion to extracellular substrates but also of intercellular adhesion and cell motility (reviewed in references 5, 6, and 32). In *Drosophila*, Rap1 mutations are associated with failures in several morphogenetic processes. Rap1 mutant embryos are defective in ventral and dorsal closure, and mesodermal precursors as well as primordial germ cells are impaired in their stereotypical migration patterns (2, 4). Thus, Rap1 is vital for various morphogenetic processes

* Corresponding author. Mailing address: Cold Spring Harbor Laboratory, 1 Bungtown Road, Cold Spring Harbor, NY 11724. Phone: (516) 367-6829. Fax: (516) 367-8815. E-mail: vanaelst@cshl.edu.

[∇] Published ahead of print on 10 September 2007.

that require cell migration and associated cell shape changes. We previously demonstrated that Rap1 relies to a large extent on its effector protein AF-6/Canoe (Cno) to mediate its action in the DC process (4). Here, we report that the exchange factor *Drosophila* PDZ-GEF (dPDZ-GEF) serves as a Rap1 activator to confer cell shape changes and to modulate cell plasticity in epithelial cells. In analyzing DC in the embryo and wing disc morphogenesis at later developmental stages, we find that dPDZ-GEF links via Rap1 to the effector protein Cno to regulate MyoII function and to generate and adjust lateral cell contractility. Thus, our data reveal a novel Rap1-dependent pathway that is critical for the maintenance and modulation of cell shape and plasticity in epithelial tissues.

MATERIALS AND METHODS

Drosophila strains and genetics. Canton S flies were used for germ line transformation and control experiments. *dPDZ-GEF* alleles were the following: *Gef26¹*, also called *l(2)k13720*, *dizzy^P*, and *pdz-gef¹* (35); *Gef26²*, also called *EP(2)0388*, *dizzy^{EP}*, and *pdz-gef²* (35) (Szeged Stock Center); *Gef26³* (57); and *Gef26^{C1}* and *Gef26^{C2}*, which were generated in this study. For the isolation of the latter mutant alleles, the *gmrGAL4* driver line was crossed to *EP(2)0388* males that had been mutagenized with 25 mM ethyl methanesulfonate. G₁ males subsequently were scored for a loss of a *gmrGAL4*>*EP(2)0388*-specific rough-eye phenotype and were mated to *Gef26¹/CyO* females for complementation testing. Positive alleles then were subjected to a second complementation cross with females carrying the *Df(2)BSC5* deficiency, which uncovers the region 26B1-2;26D1-2 (FlyBase). Other alleles used in this study were *Df(2L)BSC5* (Bloomington 6299); *cno²* and *cno^{mis1}*; *Rap1^{B3}* and *Rap1^{CD3}* (both provided by I. Harihanan); *zip¹* and *zip²* (Bloomington 4199 and 8739); and *zip^{br}* (obtained from D. Kiehart).

P-element reversion was performed with *Sp/CyO*; *Sb Δ2-3/TM6* flies as a transposase source. The following driver lines were used: *gmrGAL4* (Bloomington 321), *engrailed-GAL4* (*enGAL4*) (a gift from H. D. Ryoo), and *dPDZ-GEFGAL4* (this study; see below). Transgenes used include *UAS-2xEGFP* (Bloomington 6658); *UAS-DRap1^{V12}*, *UAS-DRap1^{WT}*, *UAS-DRap1^{N17}*, and *UAS-cno^{WT}* (4); and *UAS-dPDZ-GEF2*, *UAS-myr-dPDZ-GEF2*, *UAS-dPDZ-GEF^{EGFP}*, *UAS-dPDZ-GEF-IR*, and the genomic *dPDZ-GEF^{EGFP}* rescue construct (see below). Transgenic lines were generated by P-element-mediated transformation (48). Embryos in genetic interaction and rescue experiments were genotyped using green fluorescent protein (GFP)-expressing balancers.

Standard recombination techniques were used to generate the *FRT40A*, *Gef26¹* chromosome, and genetic mosaics were generated by FLP/FRT-mediated recombination. Clones in adult wings were induced with the *Minute* technique and were marked with *forked* using *w^{β6A} hsFLP^{1.22}; FRT40A M(2)Z f⁺* (14). Heat shocks were applied for 1 h at 37°C 4 days after egg deposition (AED). For wing disc analysis, *y w hsFLP^{1.22}; FRT40A, armLacZ*, or *y w hsFLP^{1.22}; FRT40A M(2)24 armLacZ/CyO* females were crossed to *y w; FRT40A Gef26¹/CyO* males, and 24-h egg collections were heat shocked for 30 min 3 or 4 days AED. For the generation of germ line clones (GLCs) with the dominant female sterile/FLP technique (10), *y w hsFLP^{1.22}; FRT40, Gef26³/CyO* females were mated with *w; FRT40 ovoD1* males. Recombination was induced by successive heat shocks at days 4, 5, and 6 AED. Female progeny were mated to *Df(2L)BSC5/CyO-GFP* males, and GFP-negative embryos were selected for cuticle analysis. Fly culture, crosses, and recombination techniques were performed at 25°C according to standard methods.

YTH screen. Yeast two-hybrid (YTH) screening and assaying were performed as previously described (4). A *Drosophila* embryonic cDNA library in pGAD (4) was screened in the L40 yeast reporter strain (54) using wild-type *Rap1* cloned in pBTM116 as bait.

Molecular biology. A partial cDNA clone starting at nucleotide 667 of the *dPDZ-GEF* coding sequence was isolated in a YTH screen using *Rap1* as bait. The sequence encoded an alternative exon 6, contributing the alternative C-terminal peptide sequence GPPNFMDSKCTICMPMMQ. For this variation, we termed the cDNA *dPDZ-GEF2*. The full-length cDNA of *dPDZ-GEF2* was produced by PCR from an embryonic cDNA library using 5' AAAGGAAAAAAGCGGCCGC CACCATGGATCCGTATCACCATATCAG and 3' CTAGTCTAGATTATTGA TTATGGGTGGCATGGG primers and was subcloned in pUAST to generate pUAST-*WT**dPDZ-GEF2*. pUAST-*myr**dPDZ-GEF2* was constructed by inserting the sequence encoding the first 69 amino acids of Dsrc41 upstream of the ATG start

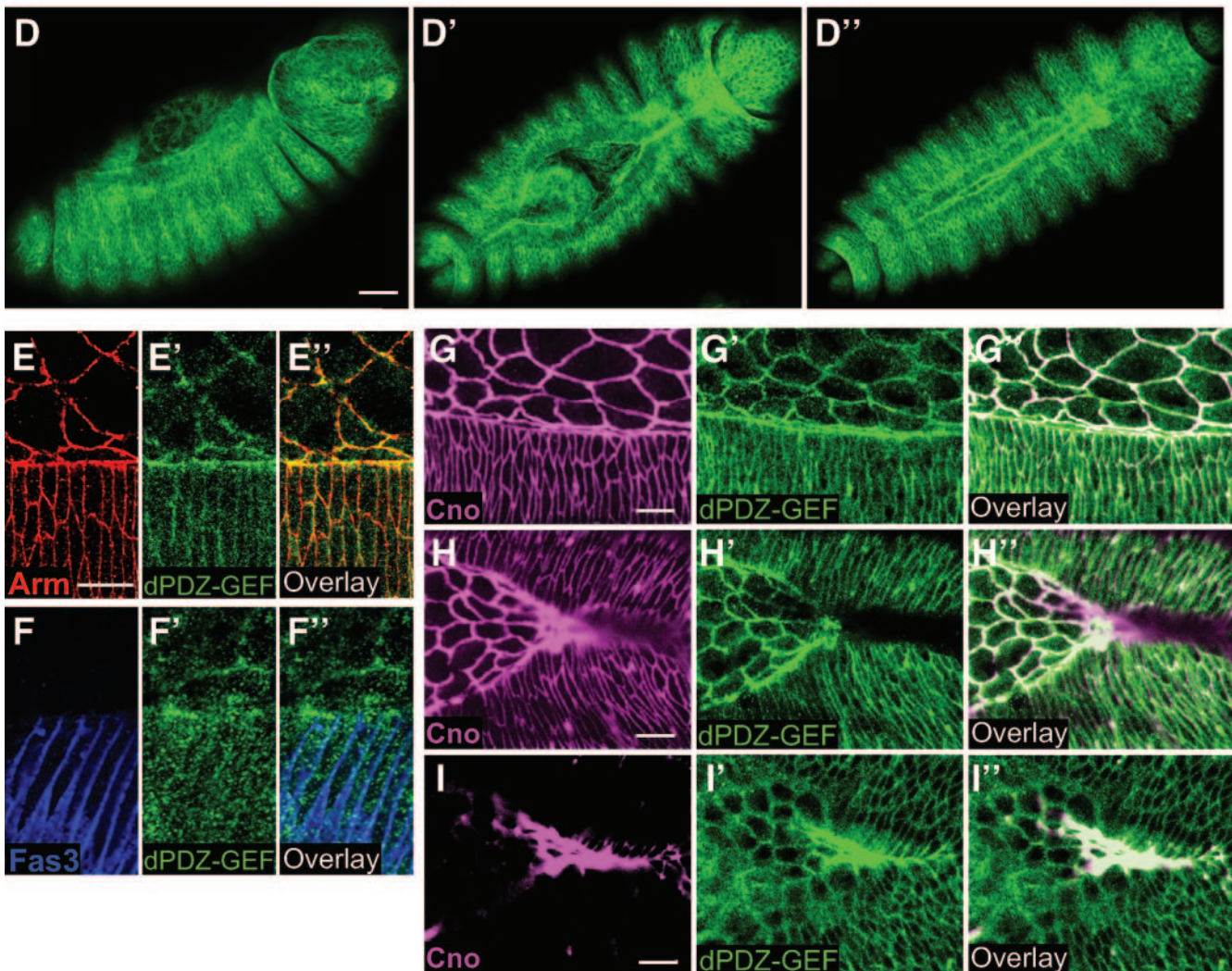
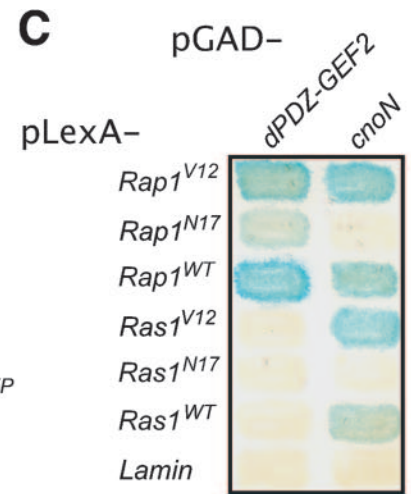
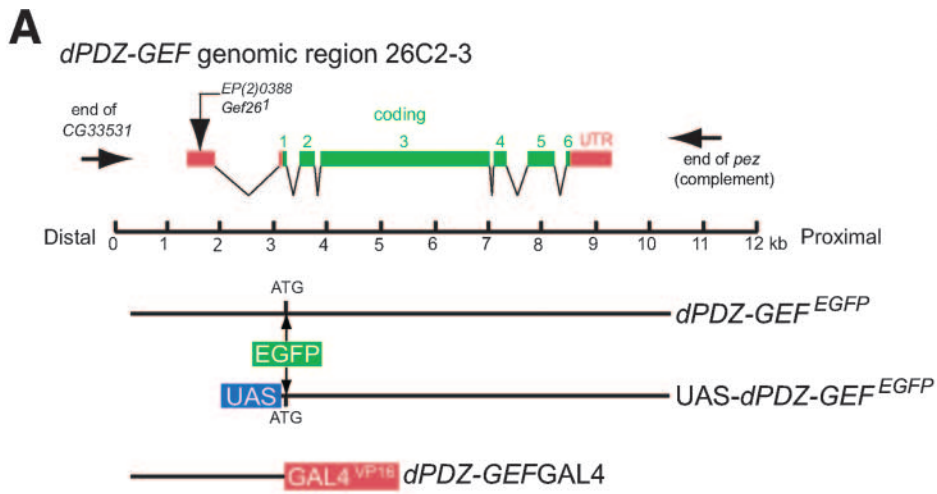
codon of dPDZ-GEF2. The genomic rescue construct *dPDZ-GEF^{EGFP}* was obtained from BAC R05J04 (RPCI-98 05J.4; Children's Hospital Oakland Research Institute) by PCR amplification and insertion into pCaSpeR4. A novel NotI site was introduced upstream of the native ATG start codon, which subsequently served to introduce an *EGFP* moiety in frame with the 5'-protein-coding region of the ATG start codon. For *dPDZ-GEFGAL4*, a *dPDZ-GEF* promoter fragment starting 2,975 bp upstream of the ATG start codon was inserted into pCaSpeR4 and C-terminally fused to the *GAL4/VPI6* transcriptional activator sequence (kindly gifted by J. Rodriguez). pUAST-*dPDZ-GEF^{EGFP}* was made by transferring the genomic sequence downstream of the ATG start codon from *dPDZ-GEF^{EGFP}* to pUAST and subsequent addition of an enhanced GFP (EGFP) tag upstream of the ATG. The YTH constructs pLexA-*Rap1^{V12}*, pLexA-*Rap1^{N17}*, pLexA-*Rap1^{WT}*, and pGAD-*cnoN* were previously described (4). pLexA-*DRas1^{V12}*, pLexA-*Ras1^{N17}*, and pLex-*Ras1^{WT}* were generated by insertion of the respective cDNAs into pBTM116 (54). For RNA interference (RNAi) purposes, the *dPDZ-GEF* coding sequence from bp 277 to 1031 was amplified with AvrII- or NheI-linked complementary primer sequence 5' AGTCTTACCGTGGCGGATGCC and XbaI-linked primer sequence 5' TCCTGCGTCTGTGCGCATCC and inserted stepwise as inverted repeats in a tail-to-tail orientation into pWIZ (36).

Immunohistochemistry. Embryos were fixed with heat/methanol (53) or 8% paraformaldehyde (25), stained with the indicated antibodies, and mounted in Vectashield medium (Vector Laboratories). Third-instar larval imaginal discs were fixed in 4% paraformaldehyde-phosphate-buffered saline. Antibodies used were the following: rat anti-Cno (1:50) (4); mouse anti-Arm (N2 7A1; 1:25) (Developmental Studies Hybridoma Bank [DSHB]); mouse anti-Dlg (4F3; 1:50) (DSHB); mouse anti-Fas3 (7G10; 1:20) (DSHB); rabbit anti-Zip/MyoII (1:800) (a gift of R. Karsess); mouse anti-β-galactosidase (1:2,000) (Sigma); rabbit anti-β-galactosidase (1:5,000) (Cappel); rabbit anti-GFP (1:500) (MBL). Alexa 594-conjugated phalloidin (Molecular Probes) was used at 2 U ml⁻¹. Alexa fluorophore-coupled secondary antibodies were from Molecular Probes and were used at 1:250. Confocal images were captured on an LSM 510 Zeiss laser-scanning microscope.

For DC survival analysis, embryos not carrying GFP-expressing balancers were selected, transferred to fresh grape plates, and aged for 36 h at 25°C. Cuticle preparations were as described in Takahashi et al. (50), and differential interference contrast images of cuticles were collected with an Axioplan 2 Zeiss microscope. Adult wings were dehydrated in isopropanol, mounted in Canada Balsam (Sigma), and digitally photographed with bright-field illumination using a Nikon SMZ microscope. For quantification, tricombe regions from five independent wings were photographed at ×40 magnification with bright-field illumination. Files were imported into the MatLab 7.1 program (Mathworks), and tricombe numbers per fixed area were counted and compiled.

RESULTS

dPDZ-GEF is expressed in the gastrulating embryonic ectoderm and colocalizes with Cno. In a previous study, we demonstrated an essential role for the Rap1/Cno GTPase/effector complex in the process of epithelial migration driving DC (4). It remained, however, unknown how Rap1 becomes activated in DC and which cellular processes Rap1/Cno signaling impinges upon. To further elucidate the signaling networks to which Rap1 is integral, we performed a YTH screen using *Rap1* as bait. This resulted in the isolation of a cDNA encoding a splice variant of the Rap exchange factor *dPDZ-GEF* or *dizzy*, which we termed *dPDZ-GEF2*. Computational sequence analysis revealed six coding exons, of which the last exon deviates from the previously described *dPDZ-GEF/dizzy* sequences (Fig. 1A; also see Materials and Methods) (22, 57). In common with the previously described protein sequences, dPDZ-GEF2 harbors a cyclic nucleotide monophosphate-binding domain, a GefN domain, a PDZ domain, and a Ras-associating (RA) domain, as well as a consensus catalytic guanine nucleotide exchange factor (GEF) domain (Fig. 1B), all of which are encoded by the third coding exon. We observed that dPDZ-GEF2 binds to the wild-type form of *Rap1* as well as to both a constitutively active (CA) and a dominant-negative



(DN) mutant form of Rap1 (Fig. 1C). The interaction with CA Rap1 is mediated by the RA domain, whereas binding to DN Rap1 occurs through the GEF domain, which carries out the nucleotide exchange reaction on Rap1 (data not shown). No interaction was detected with analogous mutants of the *Drosophila* Ras1 protein (Fig. 1C). The domain composition and Rap-binding and activation specificity are conserved among the mammalian and *Caenorhabditis elegans* homologues of the protein (12, 46). Of note, the mammalian homologue was found to reside in cell-cell junctional complexes of epithelial cells (26, 40). So far, dPDZ-GEF isoforms have been implicated in macrophage and male stem cell biology as well as in eye differentiation (22, 35, 57); however, a potential role in epithelial migration and homeostasis has not been reported.

To explore whether dPDZ-GEF plays a role in epithelial processes, we began by investigating its embryonic localization pattern. We developed a fully functional fluorescent genomic transgene, which we termed *dPDZ-GEF^{EGFP}*. Importantly, *dPDZ-GEF^{EGFP}* reverted all of the defects associated with a *dPDZ-GEF* loss-of-function (LOF) allele to wild type (Fig. 1A; also see below). When monitoring *dPDZ-GEF^{EGFP}* expression in a *dPDZ-GEF* mutant background during embryogenesis, we found that the fluorescent protein is strongly expressed in the ectoderm during cellularization and subsequently in the cellular blastoderm (data not shown). The strong presence of dPDZ-GEF^{EGFP} protein prior to the onset of zygotic transcription indicates that a large maternal component contributes to gene expression in the early embryo and may partially persist into later stages. At subsequent stages, we detected high protein levels in primordial germ cells, in the ectoderm during ventral invagination, in internalized cells that will differentiate into mesodermal and neuroectodermal structures, and in the ectodermal tissue performing the germ band elongation and retraction movements (data not shown). Of particular interest, at DC stages, during initiation, sweeping, and zippering, all epithelial tissues involved in the closure process displayed large amounts of dPDZ-GEF^{EGFP} protein (Fig. 1D to D").

Both Rap1 and Cno, the putative downstream effectors of dPDZ-GEF, are expressed at near-ubiquitous levels throughout gastrulation. Both proteins overlap in their subcellular localization patterns at the adherens junction (AJ) of cells that undergo DC (4). To trace the subcellular localization of dPDZ-GEF, we again employed *dPDZ-GEF^{EGFP}* in a mutant background. In embryos at DC stages, we observed dPDZ-GEF protein to be present at AJs of leading-edge and lateral

ectodermal cells, where it colocalizes with the β -catenin homologue Armadillo (Arm) (Fig. 1E). Moreover, we found that dPDZ-GEF codistributes with Cno at the AJ at early (stage 13) and late (stage 14) DC stages during ectodermal sweeping and suturing (Fig. 1G to I). Notably, the dPDZ-GEF protein also is detectable in more basal sections of the membrane, as demonstrated by costaining with anti-fasciclin 3 (anti-Fas3) antibodies, which decorate the lateral membrane (Fig. 1F). Overall, the distribution of dPDZ-GEF is highly reminiscent of Rap1's localization in the embryonic ectoderm (4). Thus, dPDZ-GEF, Rap1, and Cno colocalize at the AJ in the epithelial cells involved in DC, supporting the notion that they participate in a common signaling pathway.

dPDZ-GEF signals through Rap1 and Cno during DC. Our binding and protein expression data are suggestive of a scenario in which the *dPDZ-GEF* gene product functions as a relevant Rap1 activator during DC. We next sought genetic evidence of a functional pathway that links dPDZ-GEF with Rap1 signaling during DC. We made use of a P element (*Gef26¹*) that is inserted in the first untranslated exon of the *dPDZ-GEF* gene. *Gef26¹*, also termed *l(2)k13270*, represents a recessive lethal allele, and it has been associated with undetectable *dPDZ-GEF* transcript levels (22, 35, 57). To determine a role for *dPDZ-GEF* in DC, we examined the *Gef26¹* allele for phenotypic effects in the embryonic ectoderm. Thorough analysis of a *Gef26¹* mutant population ($n = 277$) revealed a significant percentage of embryos that display late gastrulation defects, ranging from a complete failure in DC (31%) to milder closure phenotypes exemplified by smaller anterior holes (29%) or the inability to invaginate the head cuticle with the adhering head skeleton (18 out of 23% of embryos with a closed cuticle) (Fig. 2C and D; Table 1). A small portion of anterior-open and -closed cuticles (5% of the total population) displayed a tail-up phenotype (Fig. 2C), indicative of a not-entirely-completed germ band retraction at the onset of DC. Seventeen percent of *Gef26¹* mutants completed embryogenesis and survived into larval stages. We found this phenotypic distribution to be closely mirrored by the *Gef26¹* allele in conjunction with the *Df(2L)BSC5* deficiency that covers the locus (Fig. 2B and Table 1). Of note, the observed phenotypic variability also has been found in mutant situations for other genes impacting DC (4, 33). One likely reason for this variability is the presence of a maternal component that varies in strength. Our analyses of *dPDZ-GEF* GLCs (see Materials and Methods) that lack maternal and

FIG. 1. dPDZ-GEF gene and protein structure and expression in the embryonic ectoderm. (A) Genomic organization of the *dPDZ-GEF* locus. *dPDZ-GEF2* contains an alternatively spliced last exon. Coding sequences are in green, and untranslated regions (UTR) are in red. Depicted underneath are the genomic regions covered by the *dPDZ-GEF^{EGFP}*, *UAS-dPDZ-GEF^{EGFP}*, and *dPDZ-GEFGAL4* transgenes. (B) The dPDZ-GEF2 protein sequence encompasses 1,569 amino acids (aa) and encodes cNMP (cyclic nucleotide monophosphate; yellow)-binding, GefN and GEF (blue), PDZ (Psd95/Dlg/ZO-1; red), and RA (green) motifs. (C) YTH interaction between dPDZ-GEF2 and Rap1 and Ras1 mutants. The L40 yeast strain was transformed with plasmids expressing dPDZ-GEF2 or an N-terminal fragment of Cno (CnoN) fused to the GAL4 activation domain (GAD) and the indicated Rap1 and Ras1 mutants, or lamin control, fused to LexA and tested for β -galactosidase activity. (D to D") Visualization of *dPDZ-GEF^{EGFP}* in a *Gef26¹* mutant background during early (D) and late (D') DC stages and zippering at the dorsal midline (D"). Scale bar, 50 μ m. (E to E") Colocalization (E") of dPDZ-GEF (E') with Arm (E) during ectodermal elongation. The dorsal side of the embryo is up. (F to F") Colocalization (F") of dPDZ-GEF (F') with Fas3 (F) in a more basal section of the ectoderm. (G to G") dPDZ-GEF (G') codistributes with Cno (G) in the lateral ectoderm and the amnioserosa at the onset of DC. An overlay is shown in panel G". (H to H") Dorsal view of an embryo late in DC in which dPDZ-GEF (H') apically colocalizes with Cno (H). An overlay is shown in panel H". (I to I") More basal sections in the confocal stack still exhibit significant dPDZ-GEF levels (I') at the membrane, while Cno (I) is absent. Sections in panels G, H, and I are 0.7 μ m thick, and the sections in panels H and I are 1.4 μ m apart. Scale bars for panels E to I", 10 μ m.

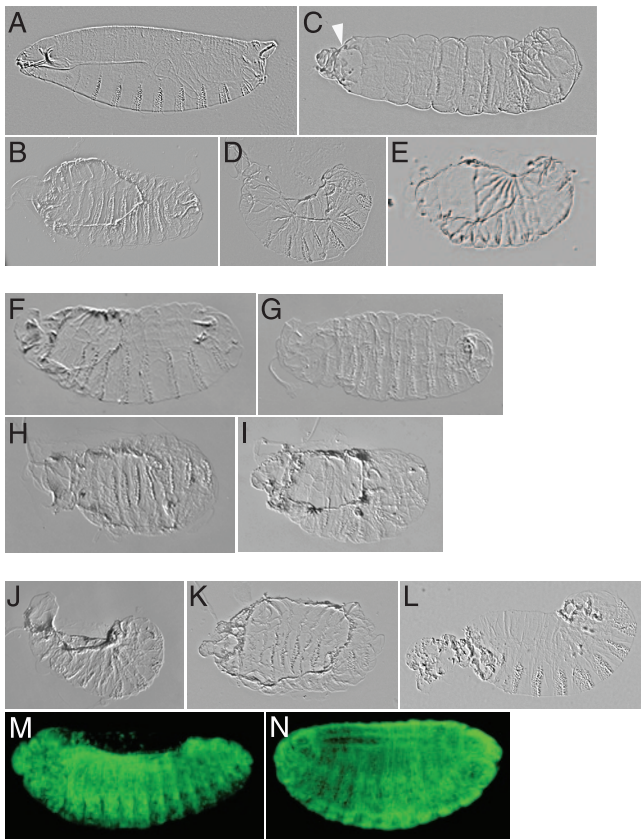


FIG. 2. *dPDZ-GEF* functions upstream of *Rap1* and *cno*. (A) Representative wild-type cuticle; (B) transheterozygous *Gef26¹/Df(2L)BSC5* cuticle; (C and D) *Gef26¹* cuticles that are (C) anterior open (the white arrowhead indicates the anterior hole) and (D) severely dorsal open; and (E) *Gef26³* germ line mutant embryo carrying a paternal *Df(2L)BSC5* deficiency. (F to I) Representative cuticles from genetic interaction experiments between *dPDZ-GEF* and *Rap1* or *cno*. Double transheterozygotes of the genotypes *Gef26^{C2}/Gef26¹; Rap1^{CD3}/Rap1^{B3}* (F); *Gef26^{C1}/Gef26¹; Rap1^{CD3}/Rap1^{B3}* (G); *Gef26^{C2}/Gef26¹; cno^{mis1}/cno²* (H); and *Gef26^{C1}/Gef26¹; cno^{mis1}/cno²* (I) show late gastrulation defects. (J to L) Representative cuticle defects investigated in epistasis tests for *dPDZ-GEF*, *Rap1*, and *cno*. (J) Dorsal-open *cno²* mutant embryo. (K) Dorsal-open *dPDZ-GEFGAL4>UAS-Rap1^{N17}* embryo. (L) Anterior-open *dPDZ-GEFGAL4>UAS-Rap1^{V12}* embryo. (M and N) Ectodermal *dPDZ-GEFGAL4>UAS-EGFP* reporter activities in early (M) and late (N) DC embryos.

zygotic expression support this notion. We found that the majority of embryos derived from these GLCs exhibit a dorsal-open phenotype (Fig. 2E and Table 1). To ascertain that the observed defects are due to the *Gef26¹* insertion and a specific obliteration of *dPDZ-GEF* gene function, we performed two additional experiments. First, we precisely excised the transposon, which resulted in a complete reversion of the DC phenotypes described above, and conferred viability to the chromosome (Table 1). Second, when a genomic rescue construct encompassing the complete *dPDZ-GEF* gene, *dPDZ-GEF^{EGFP}*, was introduced into the *Gef26¹* background, the ectodermal defects were abolished (Table 1). Together, these data indicate that *dPDZ-GEF* plays an important role in the DC process.

In subsequent experiments, we examined whether the *dPDZ-GEF* gene is indeed linked to *Rap1/Cno* signaling in

DC. Our previous study, in which we removed zygotic *Rap1* from a heteroallelic *cno* background, demonstrated a strong genetic interaction between *Rap1* and *cno* (4). Both genes provided sufficient dose sensitivity to shift the phenotypic spectrum to stronger DC defects. To assess a genetic interaction between *dPDZ-GEF* and *Rap1* and between *cno* and *dPDZ-GEF*, we generated two new hypomorphic alleles (*Gef26^{C1}* and *Gef26^{C2}*, respectively) of the *dPDZ-GEF* gene (see Materials and Methods). Both hypomorphs, when homozygous, survived into late larval stages, and embryogenesis was completed without noticeable defects. When combined with the strong *Gef26¹* allele, neither of the two hypomorphic mutations exhibited gastrulation defects, and only a small percentage of the embryos displayed embryonic lethality: 9% ($n = 278$) and 13% ($n = 264$) for *Gef26^{C1}* and *Gef26^{C2}*, respectively (see Table 1). Due to a strong maternal contribution, *Rap1* zygotic mutants are not compromised during embryogenesis and survive into larval stages (Table 1) (2, 4). However, eliminating zygotic *Rap1* expression by combining the recessive null alleles *Rap1^{CD3}* and *Rap1^{B3}* in the *Gef26^{C1}/Gef26¹* background significantly exacerbated the severity of defects. Eighteen percent of *Gef26^{C1}/Gef26¹; Rap1^{CD3}/Rap1^{B3}* embryos ($n = 212$) showed severe dorsal-open phenotypes (Table 1). Sixty-seven percent of the mutant embryos are mildly closure defective, with smaller anterior holes (Fig. 2G), and 14% have a closed cuticle. Within the latter group, 4% of the embryos were unable to involute their head skeletons. The high survival rates of *Gef26^{C1}/Gef26¹* and *Rap1^{CD3}/Rap1^{B3}* embryos (91 and 100%, respectively) were reduced to 1% in the double transheterozygotic embryos. Similar results were obtained with *Gef26^{C2}* (Fig. 2F and Table 1). We next analyzed double transheterozygotic combinations of *dPDZ-GEF* and *cno* alleles and found an even more severe distribution of late gastrulation phenotypes (Fig. 2H and I and Table 1). Sixty-nine percent and 75% of double mutant embryos (*Gef26^{C1}/Gef26¹; cno^{mis1}/cno²* and *Gef26^{C2}/Gef26¹; cno^{mis1}/cno²*, respectively) remained open, with strong ectodermal migration defects, and about a quarter of the mutant embryos exhibited weaker anterior-open defects (Table 1). Thus, allelic combinations between *dPDZ-Gef* and *Rap1* or *cno* almost entirely blocked progression into larval stages. These data indicate a remarkable degree of cooperation between all three genes in the final stages of embryonic gastrulation and support the notion that *dPDZ-Gef* acts in a common pathway with *Rap1* and *cno*.

To explore the epistatic relationships of *dPDZ-GEF* to *Rap1* and *cno*, we made use of the GAL4/UAS system (9). In order to perform a *dPDZ-GEF* tissue-specific rescue analysis, we developed a driver line by fusing a GAL4^{VP16} transcriptional activator sequence to a functional *dPDZ-GEF* promoter fragment (henceforth referred to as *dPDZ-GEFGAL4*; see Materials and Methods) and generated transgenic lines. We validated the functionality of *dPDZ-GEFGAL4*. First, GAL4 activity was strong in the lateral ectoderm throughout DC, as determined by EGFP expression (Fig. 2M and N). Second, *dPDZ-GEFGAL4* did not noticeably alter the phenotypic spectrum of *Gef26¹* mutant embryos (Table 1). Third, driving expression of a *dPDZ-GEF2* cDNA with *dPDZ-GEFGAL4* significantly alleviated the ectodermal phenotypes of *dPDZ-GEF* mutant animals (Table 1). Lastly, forced expression of DN *Rap1^{N17}* and CA *Rap1^{V12}* cDNAs with *dPDZ-GEFGAL4* gave

TABLE 1. Quantitative analysis of cuticular phenotypes of genetic interaction and rescue experiments

Genotype	Phenotype (%)				n
	Larvae hatched ^a	Cuticle closed (but with head involution defect) ^b	Cuticle partially open ^c	Dorsal open ^d	
<i>Gef26¹</i>	17	23 (18)	29	31	277
<i>Gef26¹/Df(2L)BSC5</i>	15	21 (14)	30	34	234
<i>Gef26³mat Df(2L)BSC5 pat^e</i>	0	1 (1)	48	51	138
<i>Gef26¹; Δ2-3</i>	100	0	0	0	89
<i>Gef26¹; dPDZ-GEF^{EGFP}</i>	97	3 (3)	0	0	152
<i>Gef26¹; dPDZ-GEFGAL4::UAS-dPDZ-GEF^{EGFP}</i>	89	9 (7)	2	0	170
<i>Rap1^{CD3}/Rap1^{B3}</i>	100	0	0	0	119
<i>cno^{mis¹/cno²}</i>	58	21 (12)	19	2	239
<i>Gef26^{C1}/Gef26¹</i>	91	9 (8)	0	0	278
<i>Gef26^{C2}/Gef26¹</i>	87	13 (8)	0	0	264
<i>Gef26^{C1}/Gef26¹; Rap1B^{CD3}/Rap1^{B3}</i>	1	14 (4)	67	18	212
<i>Gef26^{C2}/Gef26¹; Rap1B^{CD3}/Rap1^{B3}</i>	2	16 (9)	61	21	198
<i>Gef26^{C1}/Gef26¹; cno^{mis¹/cno²}</i>	3	1 (1)	27	69	290
<i>Gef26^{C2}/Gef26¹; cno^{mis¹/cno²}</i>	0	0 (0)	25	75	402
<i>Gef26¹; dPDZ-GEFGAL4</i>	14	18 (14)	31	37	335
<i>Gef26¹; dPDZ-GEFGAL4::UAS-dPDZ-GEF2</i>	34	51 (32)	15	0	282
<i>Gef26¹; dPDZ-GEFGAL4::UAS-Rap1^{WT}</i>	44	36 (24)	20	0	194
<i>Gef26¹; dPDZ-GEFGAL4::UAS-cno^{WT}</i>	31	43 (22)	21	5	291
<i>dPDZ-GEFGAL4::UAS-Rap1^{N17}</i>	0	0 (0)	3	97	178
<i>dPDZ-GEFGAL4::UAS-Rap1^{N17}; UAS-dPDZ-GEF2</i>	0	1 (1)	12	87	326
<i>dPDZ-GEFGAL4::UAS-Rap1^{N17}; UAS^{myr}dPDZ-GEF2</i>	0	0 (0)	8	92	166
<i>cno²; dPDZ-GEFGAL4</i>	0	5 (4)	18	77	123
<i>cno²; dPDZ-GEFGAL4::UAS-dPDZ-GEF2</i>	0	4 (4)	16	80	256
<i>cno²; dPDZ-GEFGAL4::UAS^{myr}dPDZ-GEF2</i>	0	2 (2)	16	82	280
<i>dPDZ-GEFGAL4::UAS-Rap1^{V12}</i>	0	1 (1)	63	36	120

^a The larvae hatched category did not exhibit any ectodermal defects during embryogenesis, and first-instar larvae emerged.

^b Embryos with closed cuticles did not show apparent dorsal closure defects but, as indicated in parentheses, often were head involution defective.

^c Cuticles partially open were scored as anterior closure defects that left less than a third of the embryo open.

^d Dorsal-open phenotypes were characterized by a prominent hole that encompassed more than one-third of the ectodermal surface.

^e Germ line mutant clones in which the maternal contribution was removed with the *Gef26³* allele and any paternal contribution was eliminated with the *Df(2L)BSC5* deficiency.

rise to a consistent inability to proceed through DC (Fig. 2K and L; Table 1). The fact that both DN and CA versions of Rap1 are able to halt the DC process may reflect the requirement for active cycling between the active and inactive GTPase states. Such oscillation would allow for a more flexible modulation of effector pathway activities during the different stages of ectodermal migration. Interferences by both types of dominant mutants of small GTPases have been observed in other migratory processes as well (37, 44). In sum, these observations prove the gene-specific *dPDZ-GEFGAL4* driver to be an efficient tool for the analysis of the epistatic relationships between our genes of interest. We then examined whether ectopic expression of Rap1 and Cno can alleviate the *dPDZ-GEF* LOF phenotype. Upon overexpression of Rap1, 80% of *Gef26¹* mutant embryos have a closed cuticle, with 44% proceeding into the first-instar larval stage ($n = 194$), as opposed to only 32% closed cuticles and 14% larval survival in the control *Gef26¹* mutant population ($n = 335$) analyzed in parallel (Table 1). Ectopic expression of Cno in *dPDZ-GEF* LOF mutants yielded 74% of embryos with closed cuticles and 31% surviving into larval stages ($n = 291$). In both experiments, the number of open cuticles was significantly reduced from 68% in *dPDZ-GEF* LOF embryos to 20 and 26% in *Rap1*- and *Cno*-overexpressing mutant embryos, respectively. Thus, both *Rap1* and *cno* transgenes were able to rescue the *dPDZ-GEF* LOF phenotype to a large extent. In the converse experiments, we found that ectopic expression of wild-type dPDZ-GEF2 or a myris-

toylated form of dPDZ-GEF2 had no effect on the mutant phenotype of *Rap1^{N17}* or *cno* (Fig. 2J and K; Table 1), indicating that *dPDZ-GEF* acts upstream of *Rap1* and *cno*. Together with data from our previous study demonstrating that *cno* is epistatic to *Rap1* (4), these data establish a link between the *dPDZ-GEF*, *Rap1*, and *cno* genes, with *dPDZ-GEF* acting as the most upstream element in this signaling module that promotes DC.

dPDZ-GEF promotes ectodermal cell shape changes during DC. In light of the ectodermal defects associated with the *dPDZ-GEF* LOF phenotypes at the cuticle level, we looked for cellular abnormalities in the lateral ectoderm and leading edge of mutant embryos undergoing DC. We began by analyzing the shape of cells in the lateral ectoderm of *dPDZ-GEF* mutant embryos by staining for Fas3, a lateral membrane marker. In severely compromised embryos, the lateral ectodermal cell sheets of *dPDZ-GEF* mutants displayed an inability to migrate towards the dorsal midline. This was due to a failure of ectodermal cells to elongate dorsally (compare Fig. 3A to A'). In addition, about 20% of dorsal-open animals displayed a local bunching of leading-edge cells (Fig. 3A'). We observed that local segments of the leading-edge collapse into foci and that cells in adjacent areas are abnormally extended in the anterior-posterior (A/P) direction toward the bunching regions (Fig. 3A'). Immunostaining for Arm and Cno as an AJ marker revealed similar ectodermal stretching deficiencies and local bunching defects at the leading edge (Fig. 3B' and C'), sug-

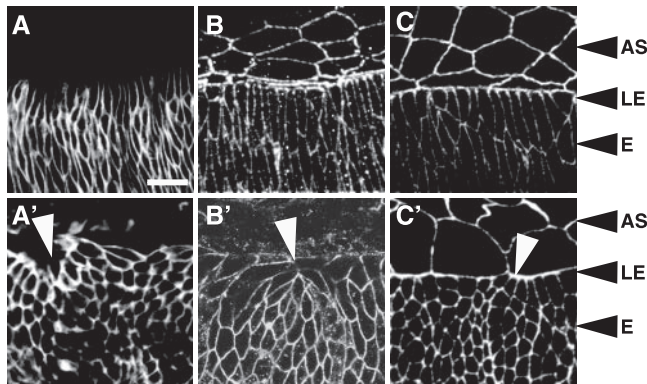


FIG. 3. *dPDZ-GEF* mutant ectoderm displays intact AJs but is characterized by cell shape abnormalities. (A and A') Wild-type (A) and *dPDZ-GEF* mutant (A') embryos immunostained for Fas3 as a lateral membrane marker. (B and B') Wild-type (B) and *dPDZ-GEF* mutant (B') embryos immunostained for Arm. (C and C') Wild-type (C) and *dPDZ-GEF* mutant (C') embryos immunostained for Cno. Note that the mutant ectoderm in panels A', B', and C' fails to elongate and that the leading-edge organization is dyscoordinated and locally contracted (see the arrowheads in panels A', B', and C'). Scale bar, 10 μ m. AS, amnioserosa; LE, leading edge; E, ectoderm.

gesting that the entire basolateral membrane compartment facing the amnioserosa is involved in this phenomenon. Notably, this phenotype also is present in embryos overexpressing a DN mutant version of *Rap1* and in embryos deficient for *cno* (4), and thus it likely represents a common regulatory defect in mutants of all three genes. Since Cno and Arm as AJ components were properly localized in *dPDZ-GEF* mutant embryos that showed impaired stretching towards the dorsal midline (Fig. 3B' and C'), we infer that AJ integrity is unperturbed in a *dPDZ-GEF* LOF situation. This is in agreement with earlier findings with *Rap1* germ line mutant embryos, in which Cno and Arm localization also remained unaffected (4).

Together, these findings indicate that *dPDZ-GEF* function is critical for bringing about the epithelial cell shape changes in the lateral ectoderm that are required to organize a coherently moving leading edge, and that the underlying mechanism does not seem to involve regulation of the levels or distribution of AJ components. Moreover, they underscore that *dPDZ-GEF*, *Rap1*, and Cno compose a module that regulates the proper dorsoventral elongation of ectodermal cells involved in DC.

Tissue integrity of the larval epithelium depends on *dPDZ-GEF* function. Our finding that *dPDZ-GEF*-deficient embryos display cell shape abnormalities raises the questions of whether these also are manifest at later stages in development and whether they can be further defined. We noted that rare homozygous *dPDZ-GEF* mutant adult escapers exhibit a marked wing phenotype, in which the wing blades are not extended in a straight fashion but bend downwards, suggesting that cell shape abnormalities might interfere with proper wing morphogenesis. Therefore, we decided to address *dPDZ-GEF* mutant situations in the wing disc epithelium at late larval stages. Analysis of the wing epithelium also provides the advantage of being able to differentiate between cell-autonomous and non-autonomous effects. We first examined *dPDZ-GEF* expression throughout disc morphogenesis. Visualizing *dPDZ-GEF*GAL4 expression with a UAS-EGFP reporter revealed high levels of

expression in the entire cephalic complex, which represents the developing epithelium in larval life (data not shown). Analysis of the wing imaginal disc showed that *dPDZ-GEF^{EGFP}* is present in all developing wing compartments, including the pouch, margin, and hinge regions (Fig. 4A). Furthermore, confocal cross-sectioning showed a marked *dPDZ-GEF* accumulation at the lateral membrane that strongly resembles the distribution of *Rap1* (Fig. 4B) (31) and a colocalization with Arm at the apical border of the lateral membrane (Fig. 4C to C'). The conservation of *dPDZ-GEF*'s subcellular localization between the embryonic ectoderm and the wing disc epithelium prompted us to perform a mosaic analysis employing the FLP/FRT system, which enables the generation of mitotic mutant clones in an otherwise wild-type epithelium (60). The clones we obtained were, however, relatively small, which impeded a detailed analysis of larger contiguous areas of mutant cells. To generate larger clones, we exploited the *Minute* technique (42). *Minute* mutations impose a growth disadvantage on wild-type cells, which often allows for clonal expansion and survival of mitotic clones into adult stages. This technique previously has been employed to define the roles of adhesion molecules and cytoskeletal regulators in wing disc morphogenesis (15, 58). We analyzed the distribution of cell-cell junctional markers and the shape of cells in clonal and surrounding wild-type tissues. Consistent with our findings for the embryo, we found that the AJ components, Arm and DE-cadherin, were evenly distributed around the circumference of *dPDZ-GEF* mutant cells (Fig. 4D to D'' and data not shown), indicating that AJ integrity is not perturbed by the loss of *dPDZ-GEF* function. However, we noticed a frequent widening of mutant cell perimeters in zones in which mutant cells contacted surrounding wild-type cells (Fig. 4D'''). In contrast, wild-type cells that border mutant clones often displayed diminished circumferences (Fig. 4D'''). When examining the more basally located septate junction (SJ), using Discs large (Dlg) as a marker, we also found that the Dlg protein is present evenly around the entire circumference of mutant cells. However, here as well we observed that mutant cell perimeters were widened to an even larger extent than that at the AJ of *dPDZ-GEF* cells bordering on wild-type tissue (Fig. 4E' and E'''). Cell circumferences were vastly extended not only at the borders of mutant clones but also in interiorly residing mutant cells (Fig. 4E'''). Wild-type cells close to the border of mutant clones, in contrast, were even more shrunken than those at the more apical AJ (Fig. 4E'''). Thus, a diminished circumference in wild-type cells contrasts with a circumferential expansion in mutant cells, which suggests a loss of contractile force around the apicolateral membrane domain in *dPDZ-GEF* mutant cells. Importantly, these effects are not due to the *Minute* background, since wild-type control clones within the same *Minute* background did not exhibit cell shape abnormalities. Neither Arm nor Dlg staining revealed any alterations in cell constriction at the clonal boundaries of wild-type control clones (Fig. 4F to G'). These findings suggest that *dPDZ-GEF* regulates lateral contractility and that its function is important for proper wing morphogenesis.

Due to the growth disadvantage of *Minute* tissue, features of mutant clones originating in the larval wing disc epithelium often survive through pupal development into the adult (42). Hence, we next surveyed adult wings for the phenotypic ex-

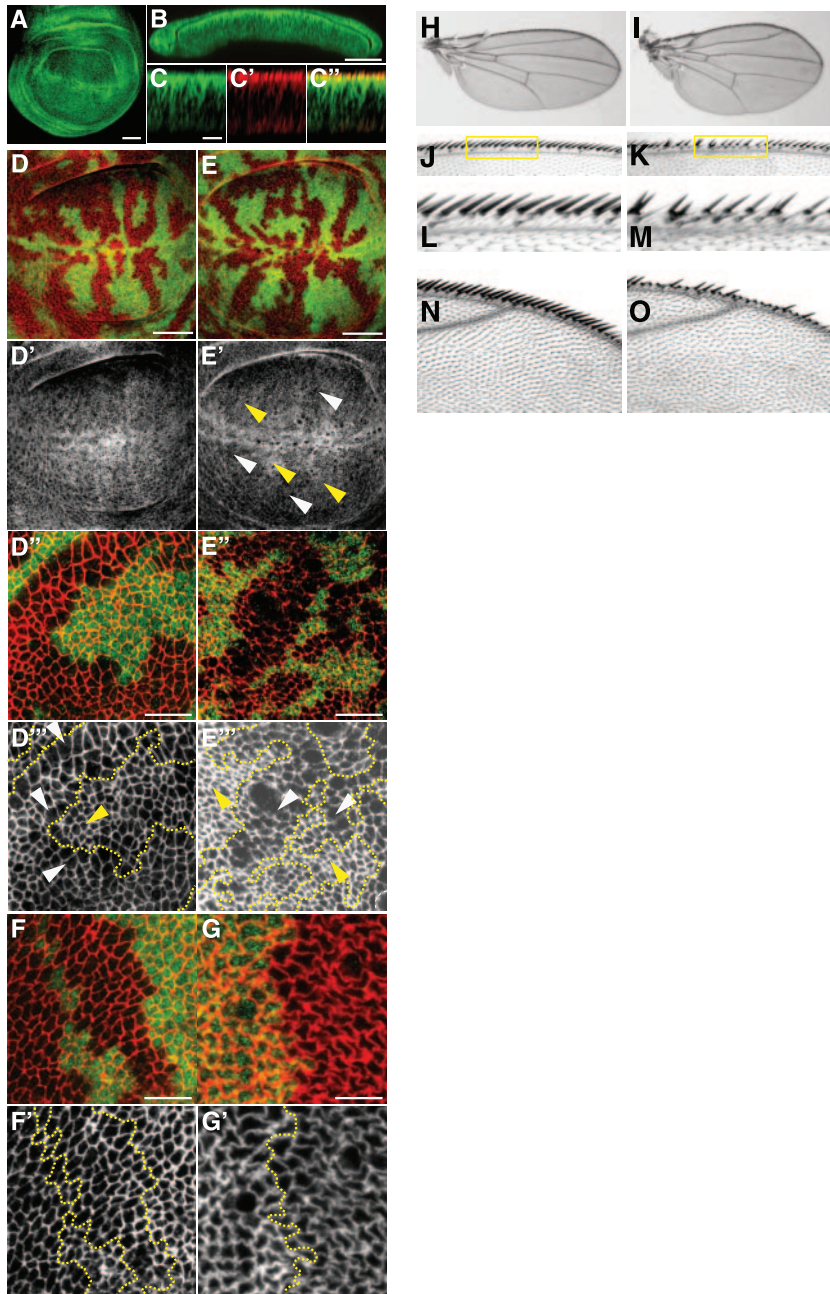


FIG. 4. Loss of *dPDZ-GEF* is associated with a reduction of apicolateral cell contractility. (A) *x-y* section through a third-instar larval *Gef26¹; dPDZ-GEF^{EGFP}* wing disc. (B) *x-z* section through a *Gef26¹; dPDZ-GEF^{EGFP}* wing disc. *dPDZ-GEF* is ubiquitously expressed throughout the epithelium. (C to C'') *x-z* sections through a *Gef26¹; dPDZ-GEF^{EGFP}* wing disc immunostained for *Arm* (C'). *dPDZ-GEF* (C) localizes to the lateral membrane and displays overlap with *Arm* staining at the AJ (C''). (D to D'') *Gef26¹ Minute⁺* mutant clones (marked by a lack of β -galactosidase expression, which labels wild-type tissue in green) immunostained for *Arm* (red in panels D and D' or white in panels D' and D''). (D'' and D''') High magnification of the region of *Gef26¹* mosaic tissue. Mutant cells bordering on wild-type areas (encircled with a dashed yellow line) are stretched (white arrowheads in panel D''), whereas more distal wild-type cells are slightly contracted (yellow arrowhead). (E to E'') *Gef26¹ Minute⁺* mutant clones lacking β -galactosidase expression (green) and immunostained with anti-*Dlg* as an SJ marker (red in panels E and E' or white in panels E' and E''). (E and E') Clonal areas are less tightly packed (white arrowheads) than adjacent wild-type areas (yellow arrowheads). (E'' and E''') High magnification of *Gef26¹* mosaic tissue stained for *Dlg*. Clonal areas (white arrowheads) display markedly widened cell perimeters compared to those of wild-type cells (yellow arrowhead). (F and F') High magnification of a *Minute* control mosaic region labeled with an anti-*Arm* antibody (red in panel F and white in panel F') and β -galactosidase expression (green) present in *Minute* mutant cells. (G and G') High magnification of the *Minute* control region immunostained with anti-*Dlg* (red in panel G and white in panel G'). Yellow lines in panels F' and G' demarcate clone boundaries. (H to M) Representative pictures of wild-type and *Gef26¹ Minute⁺* wings. (H) Wild-type control wing. (I) The *Gef26¹ Minute⁺* wing is characterized by a rounded geometry. (J to M) Magnified view of the anterior margin in wild-type (J and L) and *Gef26¹ Minute⁺* (K and M) wings. Images in panels L and M represent enlarged views of the boxed areas in panels J and K, respectively. Margin bristles in mutant areas display wider, uneven spacing or are not formed. (N and O) Tricomb fields in wild-type (N) and *Gef26¹ Minute⁺* mutant backgrounds. Mutant tricomb patterns exhibit widened spacing and lack the parallel organization visible in a wild-type wing. Scale bars in panels A, B, D, and E are 50 μ m; those in panels C, D'', E'', F, and G are 10 μ m.

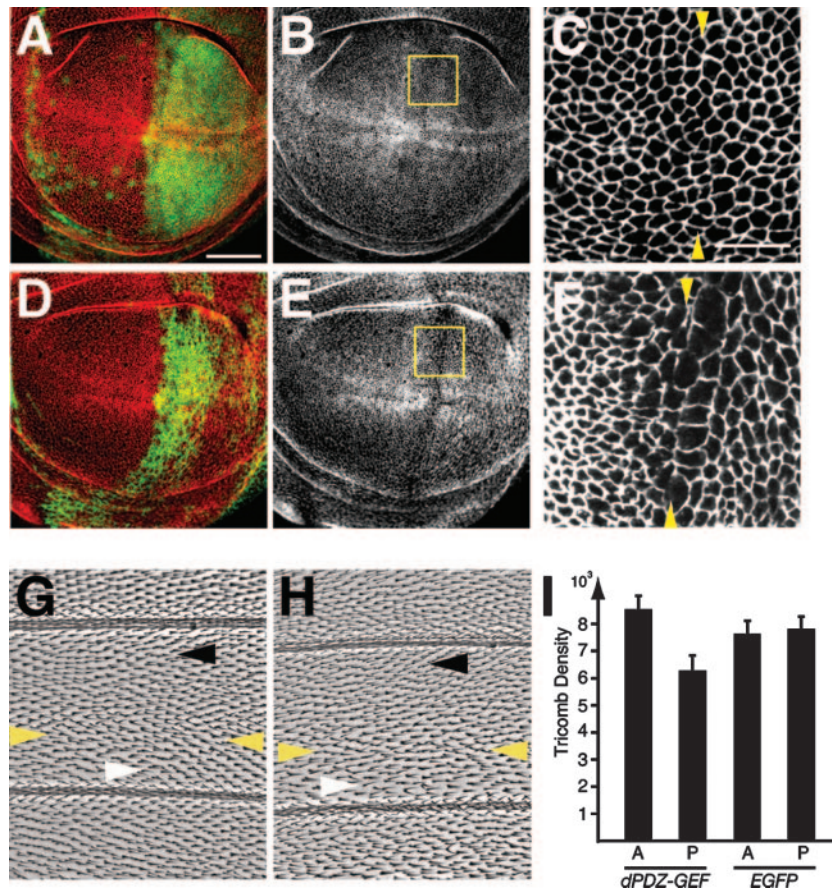


FIG. 5. Overexpression of dPDZ-GEF triggers cell shape abnormalities. (A to C) Wing pouches from third-instar larval wing discs overexpressing *EGFP* with *enGAL4*. (A) *enGAL4*>*UAS-EGFP* (green) discs were immunostained for Arm (red). (B) Arm immunostaining shown alone. (C) Enlarged view of the boxed area in panel B. Cells normally are organized along the A/P boundary (between the yellow arrowheads). (D to F) *enGAL4*>*UAS-dPDZ-GEF^{EGFP}* disc stained for Arm (red in panel D, white in panel E). (F) Enlarged view of the boxed area in panel E. Ectopic *dPDZ-GEF^{EGFP}* (green) provokes a loss of normal cell contractility along the A/P boundary (between the yellow arrows) within the posterior compartment. Anterior is left, and posterior is right. The scale bars in panels A, B, D, and E are 50 μ m, and those of panels C and F are 10 μ m. (G and H) Hair densities in *enGAL4*>*UAS-EGFP* (G) and *enGAL4*>*UAS-dPDZ-GEF^{EGFP}* (H) adult wings. Anterior is up, and posterior is down. Posterior cells of *enGAL4*>*UAS-dPDZ-GEF^{EGFP}* wings in the proximity of the A/P boundary (between yellow arrowheads) are dilated (white arrowhead in panel H) compared to those in an equivalent area of a wild-type wing (white arrowhead in panel G). As a consequence, wild-type cells facing the boundary anteriorly display a more contracted surface (black arrowheads in panels G and H). (I) Quantification of tricomb densities in wings overexpressing dPDZ-GEF^{EGFP} or EGFP with *enGAL4*. Tricomb densities were determined in the intervein region between the L3 and L4 veins anterior (A) and posterior (P) of the A/P boundary. Overexpression of dPDZ-GEF^{EGFP} with *enGAL4* decreases tricomb densities posteriorly and increases densities anteriorly; $P < 10^{-4}$ for comparisons of *enGAL4*>*UAS-dPDZ-GEF^{EGFP}* anterior to *enGAL4*>*UAS-EGFP* anterior, *enGAL4*>*UAS-dPDZ-GEF^{EGFP}* posterior to *enGAL4*>*UAS-EGFP* posterior, and *enGAL4*>*UAS-dPDZ-GEF^{EGFP}* anterior to *enGAL4*>*UAS-dPDZ-GEF^{EGFP}* posterior, whereas $P = 0.44$ for the comparison of *enGAL4*>*UAS-EGFP* anterior to *enGAL4*>*UAS-EGFP* posterior (Student's *t* tests).

pression of *dPDZ-GEF* mutant clones. We found that wings harboring multiple *dPDZ-GEF* mutant clones are more rounded and broadened than wild-type wings or wings harboring wild-type control clones (Fig. 4H and I). Each cell in the adult wing epithelium has an apically protruding hair-like structure, which in cells at the margin is a large bristle and in interiorly located cells is a smaller-sized tricomb. In wild-type wing blades, bristles and tricombs are regularly organized and spaced, the former lining the wing margin and the latter running in parallel rows through intervein regions (Fig. 4J, L, and N). *dPDZ-GEF* mutant clones display vastly disorganized bristle and tricomb patterns, with an uneven and markedly increased spacing between them (Fig. 4K, M, and O). Since the spacing between bristles and tricombs is a direct reflection of

the circumferential sizes of the cells that produce them, this phenotype is consistent with the extension of lateral cell perimeters at earlier stages during the morphogenesis of *dPDZ-GEF* mutant clones in imaginal discs and suggests difficulties in maintaining proper tissue architecture.

We reasoned that if the loss of *dPDZ-GEF* function affects cell shape and constriction, then excess amounts of dPDZ-GEF should impact the same parameters. To address this, we ectopically expressed a *UAS-dPDZ-GEF^{EGFP}* transgene (Fig. 1A) in a defined wing territory. In particular, *enGAL4* was used as a driver, which results in high levels of dPDZ-GEF expression in the posterior compartment of the wing (Fig. 5D and E). Interestingly, when staining wing imaginal discs with an antibody against Arm, we observed that dPDZ-GEF-overex-

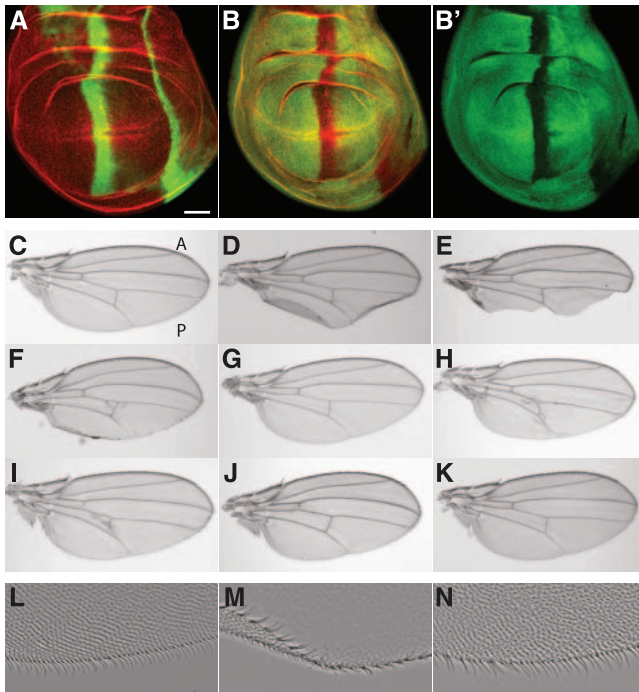


FIG. 6. *dPDZ-GEF* gain of function and LOF alter wing geometry and are modified by *Rap* and *cno*. (A) *ptcGAL4>UAS-EGFP* expression (green) along the A/P compartment boundary in a wing disc stained with an anti-Arm antibody (red). The scale bar is 50 μ m. (B and B') Expression of *UAS-dPDZ-GEF-IR* with *ptcGAL4* in a wing disc immunostained for Arm (red in panel B) eliminates the *dPDZ-GEF^{EGFP}* signal (green in panels B and B'). (C to K) Effects of modulated *dPDZ-GEF* levels in the posterior compartment of the wing. (C) Wild-type control wing. A and P indicate the anterior and posterior sides of the wing, respectively. (D and E) *enGAL4>UAS-dPDZ-GEF-IR*-expressing wings that are curled downwards with the margin folding back (D) or dorsally ruptured due to enhanced tension (E). (F) *enGAL4>UAS-dPDZ-GEF^{EGFP}*-expressing wing that shows a rounded geometry, particularly at the anterior margin and the longitudinal L2 and L3 veins. The posterior cross vein is forked at its anterior attachment site. (G) *enGAL4>UAS-dPDZ-GEF-IR/UAS-dPDZ-GEF^{EGFP}* wing. RNAi and overexpression effects ameliorate each other. (H) *enGAL4>UAS-Rap1^{WT}* wing with venation defects but intact margins and overall geometry. (I) *enGAL4>UAS-dPDZ-GEF-IR/UAS-Rap1^{WT}* wing. Ectopic levels of Rap largely rescue the *dPDZ-GEF* RNAi-specific tension defects. (J) *enGAL4>UAS-dPDZ-GEF^{EGFP/cno}* wing. Reduction of the *cno* gene dosage partially suppresses the *dPDZ-GEF* overexpression phenotypes. (K) Heterozygous *cno*² wing with a wild-type morphology. (L to N) Posterior margins of a control *enGAL4>UAS-EGFP* wing (L), a defective *enGAL4>UAS-dPDZ-GEF-IR* wing (M), and an *enGAL4>UAS-dPDZ-GEF-IR/UAS-Rap1^{WT}* wing in which the RNAi-induced defects are rescued (N).

pressing posterior cells that directly face the A/P compartment boundary are aberrantly stretched in the A/P direction (Fig. 5E and F). Importantly, overexpression of EGFP in control discs did not yield any appreciable stretching effects in posterior cells lining the A/P boundary (compare Fig. 5C to F). The *dPDZ-GEF* overexpression effect also is represented in emerging adult *enGAL4>UAS-dPDZ-GEF^{EGFP}* wings (Fig. 6F). Adult wings posteriorly overexpressing *dPDZ-GEF* assumed a more rounded geometry, with the anterior cells pulling at the posterior margin (Fig. 6F). The longitudinal veins L2 and L3 were shifted towards the anterior direction, describing a curve

instead of the relatively straight line typically observed in a wild-type wing. Furthermore, posterior tricombs close to the A/P compartment boundary displayed increased distances between each other (Fig. 5G and H). Conversely, tricombs at the opposite side of the compartment boundary were positioned much closer to each other than in a wild-type control wing (Fig. 5G and H; for quantifications, see Fig. 5I). Of note, these phenotypes differ from the ones observed for flies overexpressing growth regulators (for example, *Rheb*) in posterior cells. Growth-regulatory genes primarily alter the size of targeted wing territories without drastically affecting cell shape in adjoining territories (45). Interestingly, our data reveal that both the loss and gain of *dPDZ-GEF* function produce similar phenotypes, supporting the notion that tightly controlled cycling between active and inactive forms of Rap GTPase is important to establish tensional strength around lateral cellular circumferences.

To assess whether *dPDZ-GEF* regulates tissue organization through the Rap/Cno complex, we established a *dPDZ-GEF*-directed RNAi transgene, *UAS-dPDZ-GEF-IR* (see Materials and Methods). Before examining the effect of the RNAi transgene on wing architecture, we confirmed that it (i) was able to significantly decrease the fluorescence signal produced by *dPDZ-GEF^{EGFP}* (Fig. 6B and 6B') and (ii) could counteract the overexpression phenotype (compare Fig. 6F to G). Thus, *dPDZ-GEF-IR* was effective in knocking down *dPDZ-GEF* expression levels. We noted that expressing *dPDZ-GEF-IR* posteriorly using *enGAL4* forced the wing to round up and curl downwards (Fig. 6D), most likely as a result of a loss of lateral contractility. Two to 3 days after eclosion, wings frequently (8/32 wings) ruptured at the posterior margin (Fig. 6E). This differs somewhat from the aberrations observed in wings overexpressing *enGAL4>UAS-dPDZ-GEF^{EGFP}*, in which rupture never occurred (Fig. 6F). Bristles of *enGAL4>UAS-dPDZ-GEF-IR* wings were wider and unevenly spaced at the posterior wing margin (Fig. 6M), and in rare cases the anterior cross vein (9/32 wings) and posterior cross vein (1/32 wings) failed to form. To determine whether *dPDZ-GEF* functions in a Rap1- and Cno-dependent manner in wing development, we conducted two types of experiments. First, we tested whether concomitant overexpression of wild-type Rap1 can rescue the *enGAL4>UAS-dPDZ-GEF-IR*-associated posterior wing shape defect. While ectopic levels of Rap1 interfered with the correct establishment of posterior cross veins and occasionally interfered with that of longitudinal veins, it had no influence on the overall wing geometry, and the wing blades were extended in a straight orientation (Fig. 6H). We found, however, that Rap1 overexpression could rescue *dPDZ-GEF-IR*-induced wing bending substantially. Downward curling of the wing blades and the irregular spacing of margin bristles triggered by *dPDZ-GEF-IR* expression were largely suppressed, suggesting that these phenotypes are caused by insufficient Rap activation (Fig. 6I and N). Overexpression of Cno with *enGAL4* had lethal consequences, and no viable adults emerged. Hence, we performed an alternative interaction study in which we reduced the endogenous *cno* gene dose in an *enGAL4>UAS-dPDZ-GEF^{EGFP}* overexpression background. Removing one copy of *cno*, which by itself has no effect on wing morphogenesis (Fig. 6K), weakened the effects of *dPDZ-GEF* overexpression (compare Fig. 6F to J). Posterior cell stretching along the A/P boundary was ameliorated, and the positions of

longitudinal veins L2 and L3 shifted toward a wild-type pattern (Fig. 6J). These modifications indicate that Rap and Cno participate in the regulation of apicolateral cell constriction downstream of dPDZ-GEF. Together, our data imply that a dPDZ-GEF/Rap/Cno pathway is reiteratively used in epithelial morphogenesis to adjust apicolateral cell circumferences and cell shape in morphogenetic processes.

MyoII regulation by dPDZ-GEF signaling. Our observation that the levels and distribution of junctional components appear to be unperturbed in dPDZ-GEF LOF situations during DC and wing disc morphogenesis raises the question of which other cellular elements might be dysregulated and causative for the observed cell shape phenotypes. Increasing evidence supports the idea that contractile events in the epithelium help drive morphogenesis and that myosin proteins, particularly the nonmuscle myosin/MyoII, generate force to modulate cell shape in morphogenetic movements and in developing epithelia (13, 23). The *Drosophila* MyoII heavy chain is encoded by the *zipper* gene (*zip*) (28). It forms a dimer and, together with two essential and two regulatory light chains, constitutes a functional hexamer. In light of our observation that lateral contractility is weakened in dPDZ-GEF LOF clones, we decided to assess whether this effect is dependent on MyoII. We began by investigating the localization of MyoII in dPDZ-GEF LOF clones in wing imaginal discs by immunostaining with a MyoII-specific antibody. Strikingly, we observed that mutant cells display an abnormal, less compact organization of the MyoII network, whereas wild-type tissues surrounding mutant clones frequently exhibit foci with excessively high MyoII accumulation (Fig. 7A to B'). These differences in MyoII distribution are paralleled by the loss and gain of apicolateral constriction that we previously described (Fig. 4D''' and E'''). Thus, a failure of dPDZ-GEF mutant cells to sufficiently assemble MyoII in order to establish homeostatic contraction levels provides a likely explanation for the expansion of mutant cell perimeters and constriction in the surrounding wild-type tissue.

We then asked whether a dysregulation of MyoII also could be one of the reasons why dPDZ-GEF pathway deficiencies display DC defects. MyoII in wild-type embryos appears in a typical bars-on-a-string-type distribution on the leading edge (Fig. 7C and C'). Immunostaining of dPDZ-GEF mutant embryos, however, revealed a striking failure to assemble MyoII at the leading edge (Fig. 7D and D'). This is particularly apparent in ectodermal segments for which the leading-edge cells are stretched along the dorsoventral axis (Fig. 7E and E'). Analysis of *cno* mutant embryos showed a similar mislocalization of MyoII in leading-edge cells. *cno* mutant embryos that failed to proceed through DC often show MyoII localizing discontinuously in their leading edges (Fig. 7F and F'). These data are in agreement with earlier studies showing that compromising MyoII function prevents the proper generation of contractile forces in the leading edge and DC (13).

To obtain genetic evidence for a role of dPDZ-GEF signaling in MyoII regulation, we asked whether a concomitant reduction of gene dosages at the *zip* and dPDZ-GEF or *cno* loci would reveal genetic interactions. To this end, we made use of a transheteroallelic *zip* combination (*zip^{ebr}/zip²*) that does not provoke significant embryonic lethality (Table 2) (38). Reduced dosages of the *zip* and dPDZ-GEF (*Gef26^{C2}/Gef26¹*)

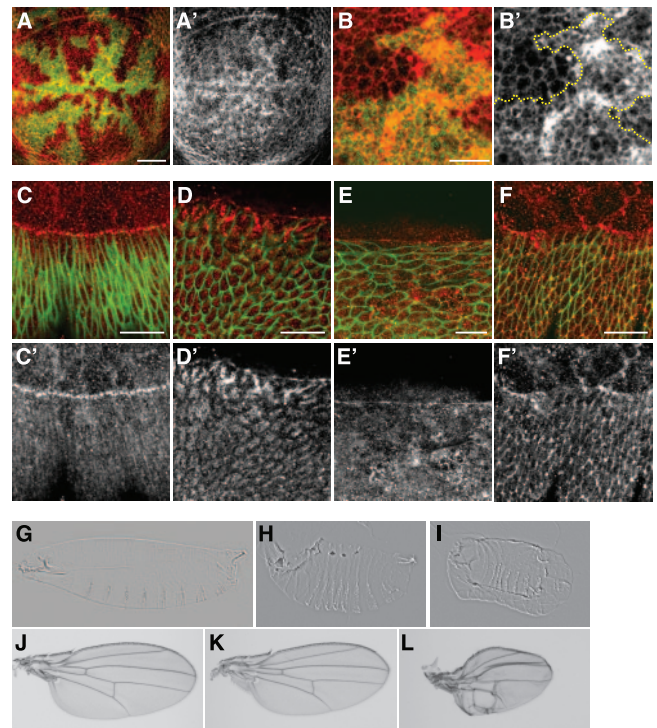


FIG. 7. dPDZ-GEF signaling is linked to MyoII function. (A and A') Wing pouch displaying *Gef26¹ Minute⁺* mutant clones (marked by a lack of β -galactosidase expression, which labels wild-type tissue in green) and immunostained with anti-MyoII (red in panel A, white in panel A'). The scale bar is 50 μ m. (B and B') High magnification of a clonal area. MyoII (red in panel B, white in panel B') is less compact in mutant tissue, whereas it is overassembled in juxtaposing wild-type tissue (green in panel B, encircled with a dashed yellow line in panel B'). The scale bar is 10 μ m. (C and C') Wild-type (C) embryo immunostained for MyoII (red) and Fas3 (green). (C') MyoII staining in white indicates the purse string formed at the leading edge (LE). (D and D') dPDZ-GEF mutant embryo immunostained for MyoII (red) and Fas3 (green in panel B, encircled with a dashed yellow line in panel B') (D) with aberrant A/P stretching of LE cells and markedly reduced accumulation of MyoII (D') at the LE. (E and E') dPDZ-GEF mutant embryo immunostained for MyoII (red) and Fas3 (green) (E). MyoII (E') does not form the wild-type bars-on-a-string pattern of MyoII at the LE and displays a distinct membrane-associated localization. (F and F') *cno* mutant embryo immunostained for MyoII (red) and Fas3 (green) (F). Ectodermal cells that initiated the elongation process still show MyoII staining (F') at the membrane but do not assemble a continuous MyoII cable at the LE. Scale bars in panels C to F are 20 μ m. (G to I) Genetic interaction between dPDZ-GEF and *cno* with *zip* during DC. (G) Wild-type cuticle. (H) *Gef26^{C2}, zip^{ebr}/Gef26¹*, and *zip²* anterior-open defects. (I) *zip^{ebr}/zip²; cno^{mis1}/cno²* dorsal-open phenotype. (J to L) Genetic interaction between a hypomorphic allelic *cno* combination and *zip^{ebr}* in the adult wing: (J) *zip^{ebr}* wing, (K) *cno^{mis1}/cno²* wing, and (L) a strongly malformed *zip^{ebr}; cno^{mis1}/cno²* wing.

genes together yielded a significant number of dead embryos (52%; $n = 248$). Six percent of the double transheterozygotic animals remained dorsal open and 25% retained anterior-open defects, while the remaining 21% proceeded through DC but did not involute their head cuticles (Fig. 7H and Table 2). Viability into the first-instar larval stage was reduced to 48%, whereas it was 93 and 87% for *zip^{ebr}/zip²* and *Gef26^{C2}/Gef26¹* embryos, respectively (Table 2). Thus, these findings indicate that the dPDZ-GEF and *zip* genes cooperate in DC. We next

TABLE 2. Quantitative analysis of cuticular phenotypes for genetic interactions of *zip* and *dPDZ-GEF* or *cno*

Genotype	Phenotype ^a (%)				<i>n</i>
	Larvae hatched	Cuticle closed (but with head involution defect)	Cuticle partially open	Dorsal open	
<i>cno^{mis1/cno2b}</i>	58	21 (12)	19	2	239
<i>Gef26^{C2}/Gef26^{1c}</i>	87	13 (8)	0	0	264
<i>zip^{ebr}/zip^{2d}</i>	93	7	0	0	90
<i>Gef26^{C2}, zip^{ebr}; Gef26¹, zip^{2e}</i>	48	21 (21)	25	6	248
<i>zip^{ebr}/zip²; cno^{mis1/cno2}</i>	5	9 (6)	57	29	93

^a Cuticle defects were categorized as described in the footnotes to Table 1.

^b Weak heteroallelic combination at the *cno* locus.

^c Weak heteroallelic combination at the *dPDZ-GEF* locus.

^d Weak heteroallelic combination at the *zip* locus.

^e In the case of the *dPDZ-GEF* interaction with *zip*, recombinant chromosomes were generated.

lowered gene dosages concomitantly at the *zip* (*zip^{ebr}/zip²*) and *cno* (*cno^{mis1/cno2}*) loci and found an even more profound effect. Embryonic lethality increased to 95%. Among them, 29% of embryos remained dorsal open and 57% remained anterior open, while 9% of embryos completed DC but did not hatch into larvae (*n* = 93) (Fig. 6I and Table 2). To analyze the interaction we observed between the *cno* and *zip* genes during DC later in wing morphogenesis, we modified the *zip* gene dose by introducing *zip^{ebr}* into the viable hypomorphic *cno^{mis1/cno2}* background. Flies carrying these genetic modifications developed malformed wings at a significant frequency (7/25 wings), while heterozygous *zip^{ebr}* and hypomorphic *cno* wings were not affected (Fig. 7J to L). Together, these data demonstrate a genetic interaction of the *zip* gene with *dPDZ-GEF* and *cno* and corroborate our immunocytochemical observations. This finding, in conjunction with the decline in lateral constriction we observed in mitotic clones and mutant embryos, compels us to propose a model in which dPDZ-GEF signaling via Rap GTPases regulates MyoII to modulate cell contractility in epithelial migration and homeostasis.

DISCUSSION

In developing tissues, Rap has been found to promote various morphogenetic processes, ranging from epithelial migration and invagination in embryogenesis to the maintenance of epithelial integrity in proliferating tissues at later stages (2, 4, 17, 31, 46). However, the mechanisms by which Rap is regulated and mediates its effects in morphogenetic episodes remain poorly understood. In this report, we delineate a pathway in which the *Drosophila* GEF dPDZ-GEF links Rap activity to MyoII and the regulation of lateral contractility and cell shape in different epithelial morphogenetic episodes.

We identified dPDZ-GEF as a putative activator of Rap GTPases in a YTH screen and subsequently demonstrated that it specifically associates with Rap, but not Ras, GTPases. PDZ-GEF is highly conserved among metazoans (12, 26, 40, 46), suggesting that it might serve common physiological roles. We found that dPDZ-GEF is highly expressed in epithelial tissues involved in embryonic DC, and, importantly, our data revealed that it functions as an activator of Rap1/Cno signaling in this process. First, as in the case of *Rap1* and *cno*, loss of zygotic *dPDZ-GEF* function is associated with an ectodermal failure, which is manifested by dorsal-open phenotypes. Eliminating both zygotic and maternal *dPDZ-GEF* elevates the frequency

of late gastrulation defects. Second, our genetic analysis places dPDZ-GEF upstream of the Rap/Cno GTPase/effector complex, as both Rap1 and Cno were able to rescue the *dPDZ-GEF* LOF phenotype to a large extent. Third, all three proteins show an overlapping localization at AJs in ectodermal cells involved in DC. Thus, our findings demonstrate that dPDZ-GEF serves as a Rap1/Cno activator to promote late epithelial gastrulation movements. In support of a conserved role of dPDZ-GEF in epithelial morphogenesis, studies with *C. elegans* demonstrated that *pxf-1*, the dPDZ-GEF homolog, is vital for epithelial integrity (46). *pxf-1* mutant animals often are confronted with hypodermal malfunctions; the underlying cellular basis of these defects, however, remains to be elucidated.

Epithelial migration processes often entail striking alterations in cell shape, and much effort has been devoted to unraveling the underlying cellular and molecular mechanisms. Our study highlights that dPDZ-GEF as a Rap activator adjusts cell shape to the demands of morphogenetic movements and imaginal disc morphogenesis. We observed that *dPDZ-GEF* mutant embryos involved in DC often exhibit bunched regions in their leading edge and an incompetence of ectodermal cells to elongate dorsally. These phenotypes also characterize embryos that either overexpress DN *Rap1* or are mutant for *cno* (4). Thus, signaling through dPDZ-GEF, Rap, and Cno (i) is vital for the organization of a coherently moving leading edge and (ii) enables the typical dorsoventral stretching of lateral ectodermal cell sheets. Our studies also unveiled a requirement for dPDZ-GEF for the adjustment of epithelial cell shape in the differentiation program of the wing imaginal disc. We found that a *dPDZ-GEF* LOF situation generated in a clonal analysis of mosaic wing discs is associated with a decline in apicolateral contractility in the vicinity of junctional complexes. Loss of contractility, as visualized by a widening of apicolateral circumferences, is coupled to a partially compensating gain of contractility in adjacent wild-type tissue. Wild-type cells in close proximity to mutant clones display smaller apicolateral circumferences. Interestingly, overexpression of dPDZ-GEF in restricted areas of the wing disc causes contractile aberrations. When ectopically expressed in the posterior compartment, dPDZ-GEF leads to a loss of apicolateral contractility in cells lining the A/P boundary. Thus, both gain and loss of *dPDZ-GEF* function compromise normal contractile strength and result in aberrant adult tissue formation. These observations suggest that a finely tuned level of Rap activation

is crucial for normal cellular and organismal development to occur. Tight requirements for activation of small GTPases *in vivo* have been documented previously, e.g., for Rho GTPases and their function in axon guidance (37). Importantly, we found in genetic modification experiments that reduced or enhanced dPDZ-GEF activity in the developing wing can be rescued by ectopic *Rap1* or lowered *cno* doses, respectively, suggesting that signaling through the dPDZ-GEF/Rap/Cno module at least partially controls disc morphogenesis. This, together with the vital cooperative roles of all three genes in embryonic cell sheet migration, corroborates the reiterative function of dPDZ-GEF/Rap/Cno signaling during epithelial development.

What are the mechanisms that translate Rap signaling downstream of dPDZ-GEF into the modulation of cell shape? Our analysis of *dPDZ-GEF* LOF situations during gastrulation and wing disc morphogenesis showed that junctional integrity is not disrupted. Both AJ and SJ belts around the apicolateral circumference are seamlessly maintained in *dPDZ-GEF* LOF tissue. However, our data support a role for the MyoII heavy chain, the product of the *zip* gene, as an effector. MyoII assembly and disassembly in migrating cells and tissue homeostasis are tightly balanced processes. In epithelial cells, MyoII localizes to cell-cell junctional complexes and is essential for establishing and maintaining intercellular adhesion and tension (16). We found that the decline in apicolateral constriction associated with *dPDZ-GEF* LOF in mitotic clones in the wing disc epithelium is accompanied by a less compact MyoII localization and that adjacent constricted wild-type cells display overassembled MyoII, which concentrates in ectopic focal structures. Also, in the DC paradigm, *dPDZ-GEF* and *cno* mutant embryos that are involved in DC exhibited failures of leading-edge cells to properly assemble MyoII. The abundant MyoII localization at the leading edge that characterizes wild-type embryos during DC is significantly diminished, and the bars-on-a-string-like MyoII distribution is lost in these mutants. In particular, regions of the leading edge adjacent to the bunched segments retain only minimal amounts of assembled MyoII. These observations strongly suggest that loss of MyoII control at the leading edge is contributing to the bunching phenotype observed in *dPDZ-GEF* and *cno* mutants. Consistent with a spatiotemporal regulation of MyoII in distinct regions of the leading edge are elegant life-imaging studies undertaken with embryos undergoing DC (13). The latter study visualized dynamic cycles of MyoII-dependent contraction and relaxation that are limited to smaller regions within the leading edge during the migration process.

In further support of the notion that dPDZ-GEF signaling acts on MyoII, we obtained evidence that *dPDZ-GEF* and *cno* genetically interact with *zip* in late gastrulation and, moreover, that *cno* is genetically linked to *zip* in wing morphogenesis. In particular, our data show a strong enhancement of dorsal-open frequencies in embryos that are double transheterozygous for hypomorphic combinations of *zip* and either *dPDZ-GEF* or *cno*. We also found that combined mutations at the *zip* and *cno* loci cause a malformation of wings. Together, our findings imply that signaling through the dPDZ-GEF/Rap/Cno module is required for MyoII function at different stages of epithelial development. Future experimentation will be required to determine the precise biochemical link between this module and

MyoII regulation. Of note, a recent study demonstrated that the mammalian Cno homolog, AF-6/Afadin, in a two-dimensional tissue culture system moves together with MyoII at the edge of wounds induced by laser ablation (51). At the onset of wound closure, a subpopulation of MyoII resides apically in the lateral membranes of cells lining the wound. However, when closure progresses into advanced stages, MyoII, together with AF-6/Afadin, migrates basalward to constrict both the wound perimeter and the apicobasal membranes facing the wound.

Our data do not rule out additional Rap effector pathways acting in synergy with Cno to bring about appropriate lateral cell contractility and MyoII regulation. The most extensively investigated signaling pathway that regulates MyoII activity in diverse systems is the Rho/Rho kinase pathway. Several studies have demonstrated that the *zip* gene exhibits strong interactions with genes encoding Rho signaling components (18, 43, 55, 59). Abundant evidence from mammalian cells indicates that Rho-stimulated Rho kinase activity leads to the phosphorylation of the regulatory myosin light chain (MLC) as well as an inhibition of MLC phosphatase, both of which in concert are stimulating MyoII assembly and contractility (1, 30). In light of recently uncovered molecular links between Rap and Rho involving Rap-associating RhoGAPs, it is an intriguing possibility that Rap is connected to Rho signaling in certain aspects of epithelial morphogenesis (34, 61). Alternatively, however, Rap could signal directly to an enzyme modifying the MyoII complex, such as kinases and phosphatases targeting MLC. Interestingly, the heavy chains of MyoII also have been reported to be subject to phosphorylation (62). Studies with chemotactic *Dictyostelium* have identified MyoII heavy-chain kinases that regulate the subcellular distribution of assembled MyoII complexes (7, 62). More recently, the Ser/Thr kinase Phg2, which acts as a potential Rap1 effector in *Dictyostelium*, also has been reported to induce MyoII heavy-chain phosphorylation (24). However, we failed to identify an obvious *Drosophila* homolog of Phg2 by extensively searching numerous databases. Future studies will be important to delineate how far Rap and Rho signaling activities are intertwined in epithelial morphogenetic events.

Our data support a model in which dPDZ-GEF, through Rap activation and MyoII regulation, contributes to the adjustment of lateral cell contractility in epithelial cells of the embryo and the developing wing. In a previous study, the analysis of *Rap1* mutant clones in the wing imaginal disc revealed a direct effect of Rap1 on the reorganization of AJs at the end of cytokinesis, where resealing of their belts has to occur between daughter cells (31). Since our data showed that AJ integrity is unperturbed in clones comprised of *dPDZ-GEF* LOF cells, we surmise that dPDZ-GEF either is not relevant for Rap1 activation in the reconstitution of a seamless AJ belt during cytokinesis or is compensated for by a still-unknown factor conferring the necessary exchange activity. On the other hand, the apicolateral constriction defects we detected as a consequence of clonal loss of *dPDZ-GEF* function so far have not been described for *Rap1* mutant clones in the same scenario. We presume either that they have escaped scrutiny or, more likely, that *Rap1* acts redundantly with its close homolog *Rap21* in adjusting apicolateral constriction, while the reorganization of AJs during cytokinesis relies solely on Rap1. In fact,

Rap1 and *Rap2l* have been shown to compensate for each other in the male stem cell niche (57). In this context, both Rap proteins cooperate downstream of dPDZ-GEF to anchor germ line stem cells to their niche. In future experiments, we plan to generate *Rap1* and *Rap2l* mitotic clones in parallel and to examine and compare their effects on cell shape and contractility.

A picture is emerging in which specialized GEFs activate Rap GTPases and selective effectors in different morphogenetic scenarios and cellular processes. For example, Rap1 signaling has been implicated in cell/extracellular matrix-dependent force transduction at focal adhesion sites of cultured cells (52). In this scenario, Rap1 is regulated by an Src/p130Cas/C3G-triggered mechanism (47). Also, apical constriction during neural tube closure in the *Xenopus* blastula has been demonstrated to depend on Rap1 function downstream of the Shroom protein (17); however, the relevant GEF in this scenario remains to be identified. The notion that Rap activation in distinct developmental processes is specified by dedicated GEFs also suggests that Rap effectors are selected in order to fulfill pathway requirements. In light of this, dPDZ-GEF and Rap1 have been implicated in the regulation of mitogen-activated protein kinase activity during differentiation of the *Drosophila* compound eye (19, 35), and a more recent study reported that D-Raf relays a signal from Rap to mitogen-activated protein kinase in Torso-receptor-dependent terminal differentiation of the early *Drosophila* embryo (41). Together, these findings suggest the possibility that dPDZ-GEF could trigger the activation of the Rap/D-Raf pathway to regulate certain differentiation processes. Our data reveal a novel function for dPDZ-GEF as an activator of Rap in the implementation of epithelial cell shape changes required for sheet migration and homeostatic cell shape maintenance in the genesis of the wing imaginal disc epithelium. We further provide evidence that Cno functions as a relevant effector of Rap downstream of dPDZ-GEF in these events and that the dPDZ-GEF/Rap/Cno module is connected to the regulation of MyoII and the generation and modulation of appropriate lateral cell contractility. Thus, our findings have unveiled a pathway linking the Rap activator dPDZ-GEF to MyoII and the regulation of lateral contractility and cell shape in epithelium migration and homeostasis. Further elucidation of dPDZ-GEF-interacting proteins and the molecular underpinnings of MyoII regulation downstream of this module in epithelial cells will be key to our understanding of these aspects of tissue morphogenesis.

ACKNOWLEDGMENTS

We thank the Bloomington and Szeged stock centers for providing *Drosophila* stocks and the DSHB for antibodies. We are indebted to D. Kiehart, R. Karess, I. Hariharan, A. Garcia-Bellido, T. Xing, H. D. Ryoo, and J. Rodriguez for kindly sharing reagents and M. Betson for critical reading of the manuscript.

This work was supported by NIH grant R01-CA096882 to L.V.A., and B.B. is a recipient of an NIH postdoctoral training grant (S T32 CA009176).

REFERENCES

- Amano, M., M. Ito, K. Kimura, Y. Fukata, K. Chihara, T. Nakano, Y. Matsuura, and K. Kaibuchi. 1996. Phosphorylation and activation of myosin by Rho-associated kinase (Rho-kinase). *J. Biol. Chem.* **271**:20246–20249.
- Asha, H., N. D. de Ruiter, M. G. Wang, and I. K. Hariharan. 1999. The Rap1 GTPase functions as a regulator of morphogenesis in vivo. *EMBO J.* **18**: 605–615.
- Baena-López, L. A., A. Baonza, and A. Garcia-Bellido. 2005. The orientation of cell divisions determines the shape of *Drosophila* organs. *Curr. Biol.* **15**:1640–1644.
- Boettner, B., P. Harjes, S. Ishimaru, M. Heke, H. Q. Fan, Y. Qin, L. Van Aelst, and U. Gaul. 2003. The AF-6 homolog canoe acts as a Rap1 effector during dorsal closure of the *Drosophila* embryo. *Genetics* **165**:159–169.
- Bos, J. L. 2005. Linking Rap to cell adhesion. *Curr. Opin. Cell Biol.* **17**:123–128.
- Bos, J. L., K. de Bruyn, J. Enserink, B. Kuiperij, S. Rangarajan, H. Rehmann, J. Riedl, J. de Rooij, F. van Mansfeld, and F. Zwartkruis. 2003. The role of Rap1 in integrin-mediated cell adhesion. *Biochem. Soc. Trans.* **31**:83–86.
- Bosgraaf, L., and P. J. van Haastert. 2006. The regulation of myosin II in Dictyostelium. *Eur. J. Cell Biol.* **85**:969–979.
- Braga, V. M., and A. S. Yap. 2005. The challenges of abundance: epithelial junctions and small GTPase signalling. *Curr. Opin. Cell Biol.* **17**:466–474.
- Brand, A. H., and N. Perrimon. 1993. Targeted gene expression as a means of altering cell fates and generating dominant phenotypes. *Development* **118**:401–415.
- Chou, T. B., and N. Perrimon. 1996. The autosomal FLP-DFS technique for generating germline mosaics in *Drosophila melanogaster*. *Genetics* **144**:1673–1679.
- Dawes-Hoang, R. E., K. M. Parmar, A. E. Christiansen, C. B. Phelps, A. H. Brand, and E. F. Wieschaus. 2005. Folded gastrulation, cell shape change and the control of myosin localization. *Development* **132**:4165–4178.
- de Rooij, J., N. M. Boenink, M. van Triest, R. H. Cool, A. Wittinghofer, and J. L. Bos. 1999. PDZ-GEF1, a guanine nucleotide exchange factor specific for Rap1 and Rap2. *J. Biol. Chem.* **274**:38125–38130.
- Franke, J. D., R. A. Montague, and D. P. Kiehart. 2005. Nonmuscle myosin II generates forces that transmit tension and drive contraction in multiple tissues during dorsal closure. *Curr. Biol.* **15**:2208–2221.
- Garcia-Bellido, A., and E. B. Lewis. 1976. Autonomous cellular differentiation of homeotic bithorax mutants of *Drosophila melanogaster*. *Dev. Biol.* **48**:400–410.
- Garcia-Bellido, A., P. Ripoll, and G. Morata. 1976. Developmental compartmentalization in the dorsal mesothoracic disc of *Drosophila*. *Dev. Biol.* **48**:132–147.
- Gibson, M. C., and N. Perrimon. 2003. Apicobasal polarization: epithelial form and function. *Curr. Opin. Cell Biol.* **15**:747–752.
- Haigo, S. L., J. D. Hildebrand, R. M. Harland, and J. B. Wallingford. 2003. Shroom induces apical constriction and is required for hinge-point formation during neural tube closure. *Curr. Biol.* **13**:2125–2137.
- Halsell, S. R., B. I. Chu, and D. P. Kiehart. 2000. Genetic analysis demonstrates a direct link between rho signaling and nonmuscle myosin function during *Drosophila* morphogenesis. *Genetics* **155**:1253–1265.
- Hariharan, I. K., R. W. Carthew, and G. M. Rubin. 1991. The *Drosophila* roughened mutation: activation of a rap homolog disrupts eye development and interferes with cell determination. *Cell* **67**:717–722.
- Hildebrand, J. D. 2005. Shroom regulates epithelial cell shape via the apical positioning of an actomyosin network. *J. Cell Sci.* **118**:5191–5203.
- Hildebrand, J. D., and P. Soriano. 1999. Shroom, a PDZ domain-containing actin-binding protein, is required for neural tube morphogenesis in mice. *Cell* **99**:485–497.
- Huelsmann, S., C. Hepper, D. Marchese, C. Knoll, and R. Reuter. 2006. The PDZ-GEF dizzy regulates cell shape of migrating macrophages via Rap1 and integrins in the *Drosophila* embryo. *Development* **133**:2915–2924.
- Jamora, C., and E. Fuchs. 2002. Intercellular adhesion, signalling and the cytoskeleton. *Nat. Cell Biol.* **4**:E101–E108.
- Jeon, T. J., D. J. Lee, S. Merlot, G. Weeks, and R. A. Firtel. 2007. Rap1 controls cell adhesion and cell motility through the regulation of myosin II. *J. Cell Biol.* **176**:1021–1033.
- Kaltschmidt, J. A., N. Lawrence, V. Morel, T. Balayo, B. G. Fernandez, A. Pelissier, A. Jacinto, and A. Martinez Arias. 2002. Planar polarity and actin dynamics in the epidermis of *Drosophila*. *Nat. Cell Biol.* **4**:937–944.
- Kawajiri, A., N. Itoh, M. Fukata, M. Nakagawa, M. Yamaga, A. Iwamatsu, and K. Kaibuchi. 2000. Identification of a novel beta-catenin-interacting protein. *Biochem. Biophys. Res. Commun.* **273**:712–717.
- Keller, R., L. A. Davidson, and D. R. Shook. 2003. How we are shaped: the biomechanics of gastrulation. *Differentiation* **71**:171–205.
- Kiehart, D. P. 1990. Molecular genetic dissection of myosin heavy chain function. *Cell* **60**:347–350.
- Kiehart, D. P., C. G. Galbraith, K. A. Edwards, W. L. Rickoll, and R. A. Montague. 2000. Multiple forces contribute to cell sheet morphogenesis for dorsal closure in *Drosophila*. *J. Cell Biol.* **149**:471–490.
- Kimura, K., M. Ito, M. Amano, K. Chihara, Y. Fukata, M. Nakafuku, B. Yamamori, J. Feng, T. Nakano, K. Okawa, A. Iwamatsu, and K. Kaibuchi. 1996. Regulation of myosin phosphatase by Rho and Rho-associated kinase (Rho-kinase). *Science* **273**:245–248.
- Knox, A. L., and N. H. Brown. 2002. Rap1 GTPase regulation of adherens junction positioning and cell adhesion. *Science* **295**:1285–1288.
- Kooistra, M. R., N. Dube, and J. L. Bos. 2007. Rap1: a key regulator in cell-cell junction formation. *J. Cell Sci.* **120**:17–22.
- Köppen, M., B. G. Fernandez, L. Carvalho, A. Jacinto, and C. P. Heisenberg.

2006. Coordinated cell-shape changes control epithelial movement in zebrafish and *Drosophila*. *Development* **133**:2671–2681.
34. **Krugmann, S., R. Williams, L. Stephens, and P. T. Hawkins.** 2004. ARAP3 is a PI3K- and rap-regulated GAP for RhoA. *Curr. Biol.* **14**:1380–1384.
35. **Lee, J. H., K. S. Cho, J. Lee, D. Kim, S. B. Lee, J. Yoo, G. H. Cha, and J. Chung.** 2002. *Drosophila* PDZ-GEF, a guanine nucleotide exchange factor for Rap1 GTPase, reveals a novel upstream regulatory mechanism in the mitogen-activated protein kinase signaling pathway. *Mol. Cell. Biol.* **22**:7658–7666.
36. **Lee, Y. S., and R. W. Carthew.** 2003. Making a better RNAi vector for *Drosophila*: use of intron spacers. *Methods* **30**:322–329.
37. **Luo, L., Y. J. Liao, L. Y. Jan, and Y. N. Jan.** 1994. Distinct morphogenetic functions of similar small GTPases: *Drosophila* Drac1 is involved in axonal outgrowth and myoblast fusion. *Genes Dev.* **8**:1787–1802.
38. **Major, R. J., and K. D. Irvine.** 2006. Localization and requirement for Myosin II at the dorsal-ventral compartment boundary of the *Drosophila* wing. *Dev. Dyn.* **235**:3051–3058.
39. **Martin, P., and S. M. Parkhurst.** 2004. Parallels between tissue repair and embryo morphogenesis. *Development* **131**:3021–3034.
40. **Mino, A., T. Ohtsuka, E. Inoue, and Y. Takai.** 2000. Membrane-associated guanylate kinase with inverted orientation (MAGI)-1/brain angiogenesis inhibitor 1-associated protein (BAP1) as a scaffolding molecule for Rap small G protein GDP/GTP exchange protein at tight junctions. *Genes Cells* **5**:1009–1016.
41. **Mishra, S., S. M. Smolik, M. A. Forte, and P. J. Stork.** 2005. Ras-independent activation of ERK signaling via the torso receptor tyrosine kinase is mediated by Rap1. *Curr. Biol.* **15**:366–370.
42. **Morata, G., and P. Ripoll.** 1975. Minutes: mutants of *drosophila* autonomously affecting cell division rate. *Dev. Biol.* **42**:211–221.
43. **Nikolaidou, K. K., and K. Barrett.** 2004. A Rho GTPase signaling pathway is used reiteratively in epithelial folding and potentially selects the outcome of Rho activation. *Curr. Biol.* **14**:1822–1826.
44. **Paladi, M., and U. Tepass.** 2004. Function of Rho GTPases in embryonic blood cell migration in *Drosophila*. *J. Cell Sci.* **117**:6313–6326.
45. **Patel, P. H., N. Thapar, L. Guo, M. Martinez, J. Maris, C. L. Gau, J. A. Lengyel, and F. Tamanoi.** 2003. *Drosophila* Rheb GTPase is required for cell cycle progression and cell growth. *J. Cell Sci.* **116**:3601–3610.
46. **Pellis-van Berkel, W., M. H. Verheijen, E. Cuppen, M. Asahina, J. de Rooij, G. Jansen, R. H. Plasterk, J. L. Bos, and F. J. Zwartkruis.** 2005. Requirement of the *Caenorhabditis elegans* RapGEF pxf-1 and rap-1 for epithelial integrity. *Mol. Biol. Cell* **16**:106–116.
47. **Sawada, Y., M. Tamada, B. J. Dubin-Thaler, O. Cherniavskaya, R. Sakai, S. Tanaka, and M. P. Sheetz.** 2006. Force sensing by mechanical extension of the Src family kinase substrate p130Cas. *Cell* **127**:1015–1026.
48. **Spradling, A. C., and G. M. Rubin.** 1982. Transposition of cloned P elements into *Drosophila* germ line chromosomes. *Science* **218**:341–347.
49. **Steimle, P. A., S. Yumura, G. P. Cote, Q. G. Medley, M. V. Polyakov, B. Leppert, and T. T. Egelhoff.** 2001. Recruitment of a myosin heavy chain kinase to actin-rich protrusions in *Dictyostelium*. *Curr. Biol.* **11**:708–713.
50. **Takahashi, K., T. Matsuo, T. Katsube, R. Ueda, and D. Yamamoto.** 1998. Direct binding between two PDZ domain proteins Canoe and ZO-1 and their roles in regulation of the jun N-terminal kinase pathway in *Drosophila* morphogenesis. *Mech. Dev.* **78**:97–111.
51. **Tamada, M., T. D. Perez, W. J. Nelson, and M. P. Sheetz.** 2007. Two distinct modes of myosin assembly and dynamics during epithelial wound closure. *J. Cell Biol.* **176**:27–33.
52. **Tamada, M., M. P. Sheetz, and Y. Sawada.** 2004. Activation of a signaling cascade by cytoskeleton stretch. *Dev. Cell* **7**:709–718.
53. **Tepass, U.** 1996. Crumbs, a component of the apical membrane, is required for zonula adherens formation in primary epithelia of *Drosophila*. *Dev. Biol.* **177**:217–225.
54. **Van Aelst, L.** 1998. Two-hybrid analysis of Ras-Raf interactions. *Methods Mol. Biol.* **84**:201–222.
55. **Verdier, V., G. C. Chen, and J. Settleman.** 2006. Rho-kinase regulates tissue morphogenesis via non-muscle myosin and LIM-kinase during *Drosophila* development. *BMC Dev. Biol.* **6**:38.
56. **Wallingford, J. B., S. E. Fraser, and R. M. Harland.** 2002. Convergent extension: the molecular control of polarized cell movement during embryonic development. *Dev. Cell* **2**:695–706.
57. **Wang, H., S. R. Singh, Z. Zheng, S. W. Oh, X. Chen, K. Edwards, and S. X. Hou.** 2006. Rap-GEF signaling controls stem cell anchoring to their niche through regulating DE-cadherin-mediated cell adhesion in the *Drosophila* testis. *Dev. Cell* **10**:117–126.
58. **Wei, S. Y., L. M. Escudero, F. Yu, L. H. Chang, L. Y. Chen, Y. H. Ho, C. M. Lin, C. S. Chou, W. Chia, J. Modolell, and J. C. Hsu.** 2005. Echinoid is a component of adherens junctions that cooperates with DE-cadherin to mediate cell adhesion. *Dev. Cell.* **8**:493–504.
59. **Winter, C. G., B. Wang, A. Ballew, A. Royou, R. Kress, J. D. Axelrod, and L. Luo.** 2001. *Drosophila* Rho-associated kinase (Drok) links Frizzled-mediated planar cell polarity signaling to the actin cytoskeleton. *Cell* **105**:81–91.
60. **Xu, T., and G. M. Rubin.** 1993. Analysis of genetic mosaics in developing and adult *Drosophila* tissues. *Development* **117**:1223–1237.
61. **Yamada, T., T. Sakisaka, S. Hisata, T. Baba, and Y. Takai.** 2005. RA-RhoGAP, Rap-activated Rho GTPase-activating protein implicated in neurite outgrowth through Rho. *J. Biol. Chem.* **280**:33026–33034.
62. **Yumura, S., M. Yoshida, V. Betapudi, L. S. Licate, Y. Iwadate, A. Nagasaki, T. Q. Uyeda, and T. T. Egelhoff.** 2005. Multiple myosin II heavy chain kinases: roles in filament assembly control and proper cytokinesis in *Dictyostelium*. *Mol. Biol. Cell* **16**:4256–4266.